



OKLAHOMA TRANSPORTATION CENTER

ECONOMIC ENHANCEMENT THROUGH INFRASTRUCTURE STEWARDSHIP

DEVELOPMENT OF AN IN SITU FATIGUE SENSOR

**J. DAVID BALDWIN, PH.D.
PRIYANTHA WIJESINGHE
SCOTT ZACHARIE
KYRAN D. MISH, PH.D.**

OTCREOS7.1-32-F

Oklahoma Transportation Center
2601 Liberty Parkway, Suite 110
Midwest City, Oklahoma 73110

Phone: 405.732.6580
Fax: 405.732.6586
www.oktc.org

DISCLAIMER

The contents of this report reflect the views of the authors, who are responsible for the facts and accuracy of the information presented herein. This document is disseminated under the sponsorship of the Department of Transportation University Transportation Centers Program, in the interest of information exchange. The U.S. Government assumes no liability for the contents or use thereof.

TECHNICAL REPORT DOCUMENTATION PAGE

1. REPORT NO. OTCREOS7.1-32-F	2. GOVERNMENT ACCESSION NO.	3. RECIPIENTS CATALOG NO.	
4. TITLE AND SUBTITLE Development of an In-Situ Fatigue Sensor		5. REPORT DATE January 2011	
		6. PERFORMING ORGANIZATION CODE	
7. AUTHOR(S) J. David Baldwin, Priyantha Wijesinghe, Scott Zacharie and Kyran D. Mish		8. PERFORMING ORGANIZATION REPORT	
9. PERFORMING ORGANIZATION NAME AND ADDRESS School of Aerospace & Mechanical Engineering The University of Oklahoma 865 Asp Avenue, Room 212 Norman, OK 73019		10. WORK UNIT NO.	
		11. CONTRACT OR GRANT NO. DTRT-06-G-0016	
12. SPONSORING AGENCY NAME AND ADDRESS Oklahoma Transportation Center (Fiscal) 201 ATRC Stillwater, OK 74078 (Technical) 2601 Liberty Parkway, Suite 110 Midwest City, OK 73110		13. TYPE OF REPORT AND PERIOD COVERED Final July 2008 - September 2010	
		14. SPONSORING AGENCY CODE	
15. SUPPLEMENTARY NOTES University Transportation Center			
16. ABSTRACT A prototype in situ fatigue sensor has been designed, constructed and evaluated experimentally for its ability to monitor the accumulation of fatigue damage in a cyclically loaded steel structure, e.g., highway bridge. The sensor consists of multiple parallel sensing arms each with a different design of notch; the arms are oriented in the direction of the primary tensile stress in the structure. When close-mounted to a steel structure, the sensor experiences the same deformation as the monitored structure and the notches localize the fatigue accumulation in the sensor and fail progressively under cyclic loading. The notches studied were of semi-circular and deep U-notch configurations. Analytical life estimates for the notched sensor arms were made based on the strain-life fatigue models, and consider several mean stress models. When compared to experimental results, the analytical life estimates consistently overestimated the notched arm lives, but were frequently of the same order of magnitude. The Morrow and Smith-Watson-Topper mean stress models performed best at capturing the experimental results. Potential explanations for the discrepancies between experiment and theory include a lack of robustness in the strain-life models when dealing with significant yielding within the notches, and machined surface finishes in the notches promoting faster fracture than was accounted for in the models. Despite the lack of comprehensive agreement in life estimates, the overall concept of a predictable, progressive failure mode for the prototype sensor was confirmed.			
17. KEY WORDS Fatigue, sensor, health monitoring, bridge, steel structure		18. DISTRIBUTION STATEMENT No restrictions. This publication is available at www.oktc.org and from NTIS.	
19. SECURITY CLASSIF. (OF THIS REPORT) Unclassified	20. SECURITY CLASSIF. (OF THIS PAGE) Unclassified	21. NO. OF PAGES 47 + covers	22. PRICE

DEVELOPMENT OF AN IN-SITU FATIGUE SENSOR

Final Report

January 2011

J. David Baldwin, Ph.D., P.E.
Associate Professor, School of Aerospace & Mechanical Engineering
Director, Dynamic Structures Sensing & Control Center

Priyantha Wijesinghe, Ph.D.
Research Associate, Civil Engineering & Environmental Science

Scott A. Zacharie, M.S.
Research Associate, Aerospace & Mechanical Engineering

Kyran D. Mish, Ph.D.
Professor, School of Civil Engineering & Environmental Science

University of Oklahoma
Norman, OK 73019

Oklahoma Transportation Center
2601 Liberty Parkway, Suite 110
Midwest City, Oklahoma 73110

ACKNOWLEDGMENTS

We would like to recognize Mr. Billy Mays and Mr. Greg Williams in the Aerospace & Mechanical Engineering Machine Shop for their help and guidance in machining the fatigue sensor prototypes and fabricating the sensor assemblies. Also, Natalie Beams, Sam Roswurm, Jose Santiago, and Matthew Walker conducted the basic material and fatigue characterization of the aluminum material used here as part of their Senior Capstone Design project in Mechanical Engineering. Finally our thanks are due to Dr. Thordur Runolfsson for his assistance in implementing the sensor monitoring circuit.

SI (METRIC) CONVERSION FACTORS

Approximate Conversions to SI Units				
Symbol	When you know	Multiply by	To Find	Symbol
LENGTH				
in	inches	25.40	millimeters	mm
ft	feet	0.3048	meters	m
yd	yards	0.9144	meters	m
mi	miles	1.609	kilometers	km
AREA				
in ²	square inches	645.2	square millimeters	mm ²
ft ²	square feet	0.0929	square meters	m ²
yd ²	square yards	0.8361	square meters	m ²
ac	acres	0.4047	hectares	ha
mi ²	square miles	2.590	square kilometers	km ²
VOLUME				
fl oz	fluid ounces	29.57	milliliters	mL
gal	gallons	3.785	liters	L
ft ³	cubic feet	0.0283	cubic meters	m ³
yd ³	cubic yards	0.7645	cubic meters	m ³
MASS				
oz	ounces	28.35	grams	g
lb	pounds	0.4536	kilograms	kg
T	short tons (2000 lb)	0.907	megagrams	Mg
TEMPERATURE (exact)				
°F	degrees Fahrenheit	(°F-32)/1.8	degrees Celsius	°C
FORCE and PRESSURE or STRESS				
lbf	poundforce	4.448	Newtons	N
lbf/in ²	poundforce per square inch	6.895	kilopascals	kPa

Approximate Conversions from SI Units				
Symbol	When you know	Multiply by	To Find	Symbol
LENGTH				
mm	millimeters	0.0394	inches	in
m	meters	3.281	feet	ft
m	meters	1.094	yards	yd
km	kilometers	0.6214	miles	mi
AREA				
mm ²	square millimeters	0.00155	square inches	in ²
m ²	square meters	10.764	square feet	ft ²
m ²	square meters	1.196	square yards	yd ²
ha	hectares	2.471	acres	ac
km ²	square kilometers	0.3861	square miles	mi ²
VOLUME				
mL	milliliters	0.0338	fluid ounces	fl oz
L	liters	0.2642	gallons	gal
m ³	cubic meters	35.315	cubic feet	ft ³
m ³	cubic meters	1.308	cubic yards	yd ³
MASS				
g	grams	0.0353	ounces	oz
kg	kilograms	2.205	pounds	lb
Mg	megagrams	1.1023	short tons (2000 lb)	T
TEMPERATURE (exact)				
°C	degrees Celsius	9/5+32	degrees Fahrenheit	°F
FORCE and PRESSURE or STRESS				
N	Newtons	0.2248	poundforce	lbf
kPa	kilopascals	0.1450	poundforce per square inch	lbf/in ²

TABLE OF CONTENTS

LIST OF FIGURES	vii
LIST OF TABLES	viii
EXECUTIVE SUMMARY	ix
1.0 INTRODUCTION	1
2.0 BACKGROUND	1
3.0 TECHNICAL APPROACH	3
4.0 FATIGUE SENSOR PROTOTYPE DESIGN AND PERFORMANCE	4
4.1 PROOF-OF-CONCEPT SENSOR	4
4.1.1 Experimental Program	4
4.1.2 TFTS Life Simulation	6
4.1.3 Sensor Fatigue Life Estimates	9
4.1.4 Comparison of Theory and Experiment	13
4.2 PROTOTYPE FATIGUE SENSOR PERFORMANCE	17
4.2.1 Deep U-Notch Sensor Design and Testing	17
4.2.2 Fatigue Sensor Model Simulation	21
4.2.3 Comparison of Results	28
5.0 CONCLUDING REMARKS	37
6.0 IMPLEMENTATION AND TECHNOLOGY TRANSFER	37
7.0 REFERENCES	38

LIST OF FIGURES

Figure 1: Cracked girder in Yellow Mill Pond Bridge, Connecticut [9]	3
Figure 2: Web gap cracking at end of transverse connection plate [9].....	3
Figure 3: Tensile Fatigue Test Specimen (TFTS) [all dimensions in inches]	5
Figure 4: MTS Tensile Fatigue Specimen Test Setup	6
Figure 5: ANSYS TFTS Model	7
Figure 6: ANSYS Mesh for TFTS Model.....	7
Figure 7: ANSYS TFTS Model; Y-Axis Normal Stress	9
Figure 8: Stress Concentration Factors for Shallow U-shaped Notches [13].....	11
Figure 9: Experimental vs. Theoretical Life - Morrow Criterion	15
Figure 10: Experimental vs. Theoretical Life - M-H Criterion	16
Figure 11: Experimental vs. Theoretical Life - SWT Criterion.....	16
Figure 12: Fatigue Sensor Type 2A Geometry [All Dimensions in Inches].....	18
Figure 13: Fatigue Sensor Type 1B Geometry [All Dimensions in Inches].....	19
Figure 14: Close Up of Mounted Fatigue Sensor	20
Figure 15: Dummy Fatigue Sensor Test Specimen Schematic.....	21
Figure 16: ANSYS Mesh for 2A FS Geometry	23
Figure 17: ANSYS Mesh for 1B FS Geometry	24
Figure 18: ANSYS 2A FS Model Y-Axis Normal Stress Close up 0.40 mm (1/64 inch) Notch. 26	26
Figure 19: Stress Concentration Chart for Opposed U-Shaped Notches [13]	27
Figure 20: Geometry Basis for Opposite U-Shaped Notches [13]	27
Figure 21: Fatigue Life of the 1.59 mm (1/16 inch) Notch Radius	30
Figure 22: Fatigue Life of the 0.79 mm (1/32 inch) Notch Radius	31
Figure 23: Fatigue Life of the 0.40 mm (1/64 inch) Notch Radius	32
Figure 24: Fatigue Life of the 1.02 mm (0.04 inch) Notch Ligament	33
Figure 25: Fatigue Life of the 0.89 mm (0.035 inch) Notch Ligament	34
Figure 26: Fatigue Life of the 0.76 mm (0.03 inch) Notch Ligament	35
Figure 27: Comparison of experimental notch life and estimated carrier life for constant amplitude loading	36

LIST OF TABLES

Table 1: Finite Element Mesh Parameters for TFTS	8
Table 2: Nominal Stresses Found from ANSYS TFTS Model, MPa (psi).....	8
Table 3: Sensor Material Properties [12, 11].....	10
Table 4: Tensile Fatigue Test Specimen Stress Concentration Factors	12
Table 5: ANSYS Calculated Tensile Fatigue Test Specimen Stress Concentration Factors.....	12
Table 6: Stress Concentration Factors Found from ANSYS and <i>Kt</i> Chart.....	13
Table 7: Tensile Fatigue Test Specimen Experimental Results.....	14
Table 8: Tensile Fatigue Test Specimen Theoretical Model Simulation Results.....	14
Table 9: Test Loading Conditions.....	20
Table 10: Measured Peak Strains and Calculated Displacements	22
Table 11: Finite Element Mesh Parameters for ANSYS FS Model	24
Table 12: Nominal Stresses Found from ANSYS FS Model MPa (psi).....	25
Table 13: U-Shaped Notch Geometry Parameters for 2A and 1B FS	28
Table 14: Fatigue Sensor Stress Concentration Factors	28
Table 15: Model 2A Experimental Cycles to Failure	29
Table 16: Model 1B Experimental Cycles to Failure	29

EXECUTIVE SUMMARY

Fatigue in metallic materials such as steels and aluminums can be understood as damage that is accumulated from cyclic loading. Engineered structures such as bridges and aircraft undergo cyclic loading conditions on a daily occurrence. As time progresses, fatigue damage begins to build in these structures and if proper maintenance and inspection is not performed, catastrophic failure can occur. Among nondestructive evaluation techniques, visual inspection is a common method used for evaluating the health of bridge infrastructures. The problem with visual inspection methods and fatigue damage is that fatigue damage may not always be visible until it is too late. In this study, two fatigue sensors were developed to experience the deformations of an underlying structure undergoing constant amplitude cyclic loading conditions. Our sensor consists of multiple parallel sensing arms, aligned with the tensile load direction, each having different sharp notches. The sensor is close-bonded to the monitored structure and shares the deformation characteristics of that structure. Deformations induced in the sensor cause the fatigue sensor arms to experience progressive sequential failure of the notched arm geometries as cyclic loading induces damage in the sensor. The cycle counts to failure in the sensor arms can be mapped to the fatigue damage accumulated in the underlying structure using a strain-life fatigue model.

A model simulation using finite element analysis and the strain-life fatigue approach was done to obtain the theoretical behavior of the fatigue sensors which was compared to the actual results obtained from experimental testing. This comparison revealed inconsistencies in life estimates of the sensor arms relative to the fatigue models employed. We found that no single fatigue model represented the experimental data across all load levels. The theoretical lives consistently overestimated the experiments. One potential shortcoming in the theoretical life estimates is the very large stresses experienced within the sensor arm notches, typically exceeding the yield strength of the material. Such through-section yielding is clearly not well modeled by the existing theories. Also, the surface finish in the notches themselves could be playing a role in the observed fatigue lives significantly less than theory predicts.

The results obtained in this study shed valuable light on the behavior of parallel notched arm fatigue sensors. While the comparison between experiment and theory was not fully consistent across the life range, the overall trends in life prediction were promising and reaffirm the possibility of constructing sensors of this type capable of tracking the damage accumulation in metal structures.

1.0 INTRODUCTION

Structural components that operate in dynamic load environment serving critical applications require continuous monitoring as well as appropriate maintenance procedures. Some of the examples include bridges under varying moving loads, aircraft takeoff and landing, marine structures under sea waves, critical nuclear power plant applications, etc. Currently the majority of structural health monitoring (SHM) systems consist of a scheduled inspections basis and progress is underway to implement an efficient automated form of condition-based maintenance.

Fatigue damage has been identified as a threat to bridge safety. Fatigue cracks usually occur at stresses lower than the anticipated design stress levels. Unlike yielding or corrosion, fatigue cracks are seldom visible enough to be detected by visual inspection and therefore can be easily overlooked. Since a larger portion of the life of a structure is spent on crack nucleation (as opposed to crack propagation), it is vital to develop methods to detect fatigue crack nucleation.

Unfortunately, most of the methods that are developed to detect fatigue cracks do not accommodate crack nucleation and are not sensitive enough to detect it. A prototype in-situ fatigue sensor has been developed in this project to detect nucleation of fatigue damage in steel highway bridges. A combination of experimental, computational, and theoretical approaches have been employed in the design and performance testing of the prototype fatigue sensor.

2.0 BACKGROUND

The issue of monitoring structural integrity becomes crucial when structural members of interest have been subjected to patch-type repairs in lieu of costly replacements. The boron/epoxy patches [1] that are presently applied to repair cracked aircraft skins need to be progressively monitored since the epoxy interface may weaken over time. Acellent Technologies has developed a sensor called SMART Layer [2, 3] that is made of piezoelectric sensors/actuators. They also developed a diagnostic system to monitor multi-crack growth at riveted lap joints [4]. Vodicks [5] discussed the use of PVDF (polyvinylidene fluoride) piezoelectric strain sensors to monitor similar bonded composite patches. Boeing, under USAF contract [6], has developed a damage acquisition unit called the damage dosimeter to identify the frequency and temperature associated with the maximum strain activity so as to optimize the damping efficiency.

Various approaches are available today to monitor structural integrity such as X-rays, acoustic, ultrasonic, magnetic and thermal field methods, eddy-current, etc. All these approaches usually include extensive instrumentation set-up that limit their use as a stand-alone maintenance procedure, especially on structures that are in continuous use. Among the earlier methods of damage detection in simple structures, vibration related damage detection based on modal methods attracted many researchers. However later researchers such as Banks et al., [7] have shown that modal methods yield unreliable damage assessment for variable material parameters such as composites. They have proposed a non-modal NDE method to identify the spatially dependent dynamic parameters of piezoceramic structures. A literature survey of structural

health monitoring using vibration techniques was produced by Los Alamos National Laboratory [8].

In the realm of steel bridges, fatigue of the metal structural elements is one of the most pernicious failure modes in that its early stages are invisible and not easily detected by non-destructive means. If we broadly divide the continuum of the fatigue process, beginning with an undamaged, pristine structure, and progressing to a fracture condition, into crack nucleation, crack propagation, and final fracture processes, the crack nucleation portion of the life is by far the most difficult to monitor. The fatigue sensor prototype developed in this project is intended to monitor this portion of a structure's life.

According to Fisher, et al. [8], fatigue damage to steel bridges occurs mainly due to the following reasons:

1. Flaws in fabricated steel structures such as fillet welded details: Partial penetration, porosity or inclusions, lack of fusion and undercut may lead to fatigue cracks.
2. Material flaws during fabrication: Material flaws may occur as a consequence of the manufacturing process and fabrication process of steel. In rolled shapes, flaws can occur from surface and edge imperfections, irregularities in mill scale, laminations and from mechanical notches due to handling, straightening, cutting and shearing.
3. Mechanical details: Mechanical details, such as drilled holes or punched holes, are prone to severe fatigue life compared to the bare rolled shape. Furthermore, punched holes are considered to give lower fatigue life than drilled, sub-punched or reamed holes because of the edge imperfections that occur during the punching process.

Overall, the fatigue life of a steel structure is determined by three factors, (a) the number of cycles of loading to which the member is subjected; (b) the type of detail under examination; and (c) the stress range at the location of the detail.

According to Fisher [9], fatigue damage to steel bridges can be categorized mainly into 1) load induced fatigue damage, and 2) distortion induced fatigue damage.

Dynamic stresses acting on the above mentioned defects may lead to fatigue cracking of the associated members. It is assumed that these stresses can be calculated and that the loads are the same as those indicated in the strength design of the members [8]. Such damage associated with loads is called load-induced damage, e.g., Figure 1.

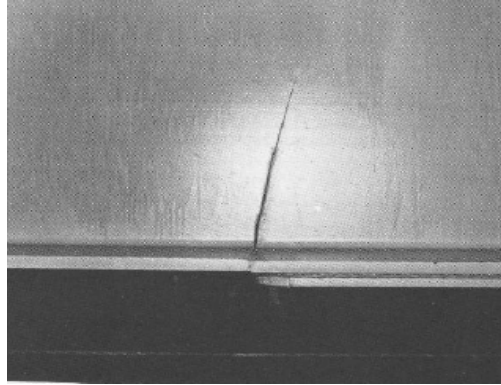


Figure 1: Cracked girder in Yellow Mill Pond Bridge, Connecticut [9]

In some cases, fatigue damage may occur as a result of imposition of deformations, not necessarily due to loads. This type of fatigue damage, which is called distortion-induced cracking, arise as a result of relatively small out-of-plane deformations in local regions [8]. This type of damage is mostly found in small web gaps and in different types of bridges such as suspension bridges, plate girder bridges, truss bridges, box girder bridges etc. It is important to know that this type of fatigue crack usually develops in planes parallel to the load-induced stresses and that after adequate flexibility is gained, these cracks may slow down or even stop. Therefore, distortion-induced damage is considered as less severe than load-induced damage. Figure 2 shows an example of distortion-induced fatigue damage.



Figure 2: Web gap cracking at end of transverse connection plate [9]

3.0 TECHNICAL APPROACH

Our goal in this project was to design, implement, and evaluate the performance of an in-situ (i.e., mounted upon the structure being monitored) fatigue sensor. The sensor consists of multiple sensing arms, mounted parallel to the primary tensile axis of the monitored structure, with notches of varying geometry in the arms. By close mounting the sensor to the structure, it was anticipated that the sensor would experience the same strains as the structure, but would accumulate fatigue damage at a much higher rate by virtue of the notches. Carefully designed notches would fail at progressively larger numbers of load cycles, and the notch failures could be correlated with the accumulation of a known amount of fatigue damage in the monitored

structure. Besides the geometric design of the sensor itself, it was the scaling between the behavior of the sensor notches and the monitored structure that would make the sensor useful in tracking damage accumulation.

4.0 FATIGUE SENSOR PROTOTYPE DESIGN AND PERFORMANCE

The development effort for the fatigue sensor followed a phased approach where a proof-of-concept specimen was developed and evaluated for its ability to deliver predictable, progressive failure of the sensing arms under cyclic load. Once that was completed, we conducted a more detailed design study considering a variety of sensor notch geometries, resulting in the final prototype characterized by the deep U-notches in the sensing arms. [10, 11]

4.1 PROOF-OF-CONCEPT SENSOR

A tensile fatigue test characterization was performed to see if progressive sequential failure could be accomplished using notched arm geometries. When notched geometries are present in a material or structure, the fatigue life can be reduced substantially when compared to the un-notched geometry configuration. These notches create localized stress concentrations in the material or structure. The results obtained from the tensile fatigue tests were analyzed and compared with the calculated theoretical results.

4.1.1 Experimental Program

The specimens used for the tensile fatigue tests were made of 7075 T6 aluminum. The specimen geometry was developed using 3-D CAD software and then machined using a CNC mill. The parameters used for the tensile fatigue test specimen (TFTS) were to maintain a constant notch ligament length of 1.3 mm (0.05 inch) and to vary the notch radius in each of the four specimen sensor arms. The notch radii used were 25.4 (1.0 inch), 19.0 (0.75), 12.7 (0.50), and 6.4 mm (0.25 inch). Overall size of the specimen was $305 \times 76 \times 1.6$ mm ($12 \times 3 \times 0.063$ inch). Figure 3 below gives an accurate representation of the TFTS geometry

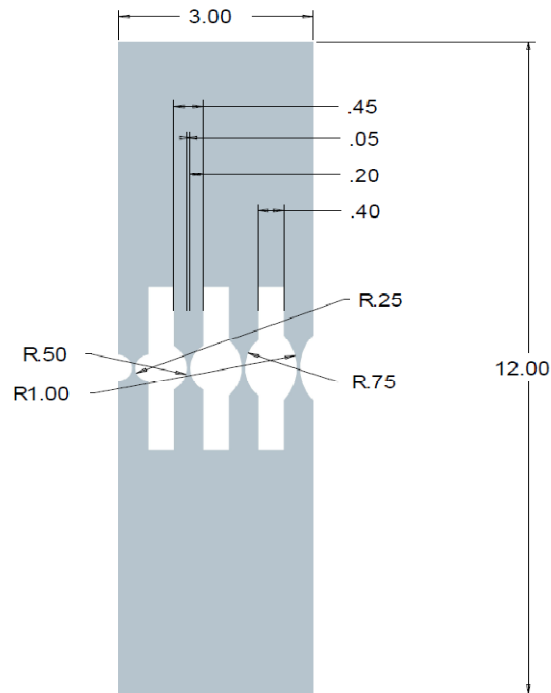


Figure 3: Tensile Fatigue Test Specimen (TFTS) [all dimensions in inches]

Cyclic load testing was performed using a MTS servohydraulic testing machine, Figure 4. The TFTS was placed in the MTS grips 38 mm (1.5 inch) from the top and the bottom so the actual specimen dimensions experiencing fatigue loading cycles was $229 \times 76 \times 1.6$ mm ($9 \times 3 \times 0.063$ inch). A total of eleven TFTS test specimens were manufactured. The test was setup to run under sinusoidal displacement control with 0.51 mm (0.02 inch) maximum displacement and 0.25 mm (0.01 inch) minimum displacement. The test was run under an excitation frequency of 1 Hz.



Figure 4: MTS Tensile Fatigue Specimen Test Setup

4.1.2 TFTS Life Simulation

A finite element-based model simulation of the TFTS was performed to obtain the estimated number of cycles to failure based on strain-life fatigue theory. A finite element model was developed in ANSYS Workbench and used to estimate the nominal stresses present in the TFTS under tensile loading. These stress results were input to a strain-life fatigue analysis code developed in MATLAB to estimate the number of cycles to failure.

The TFTS model in ANSYS was setup to mimic the experimental testing of the TFTS. The TFTS was partitioned into three sections to allow the proper application of boundary conditions. The lower and upper tabs had dimensions $38 \times 44 \times 1.6$ mm ($1.5 \times 1.75 \times 0.063$ inch) and the middle section had dimensions $229 \times 76 \times 1.6$ mm ($9 \times 3 \times 0.063$ inch), Figure 5. In the ANSYS model the lower tab was given a fixed boundary condition disabling any movement in the x -, y -, and z -directions; the upper tab was given a displacement boundary condition only allowing movement in the y -axis (tensile) direction. A frictionless support was applied to the outer surfaces (surface normal to the top and bottom surfaces) of the middle section.

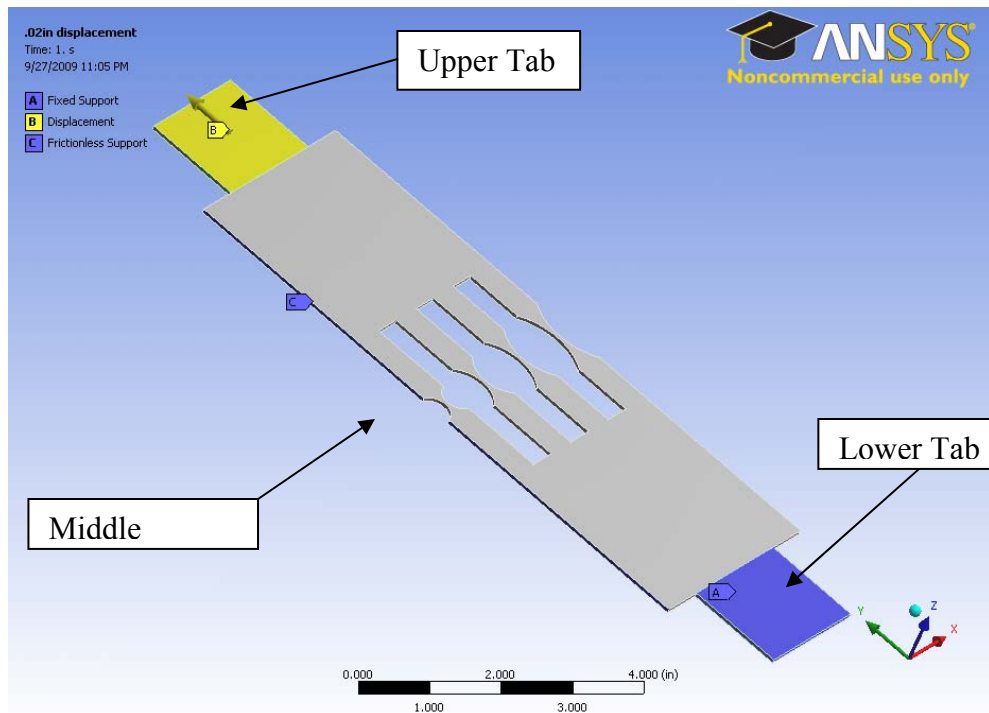


Figure 5: ANSYS TFTS Model

The mesh for the TFTS in the ANSYS model (Figure 6) was refined at the nominal stress and notch locations to capture the higher stress gradients in those positions; the mesh statistics are given in Table 1.

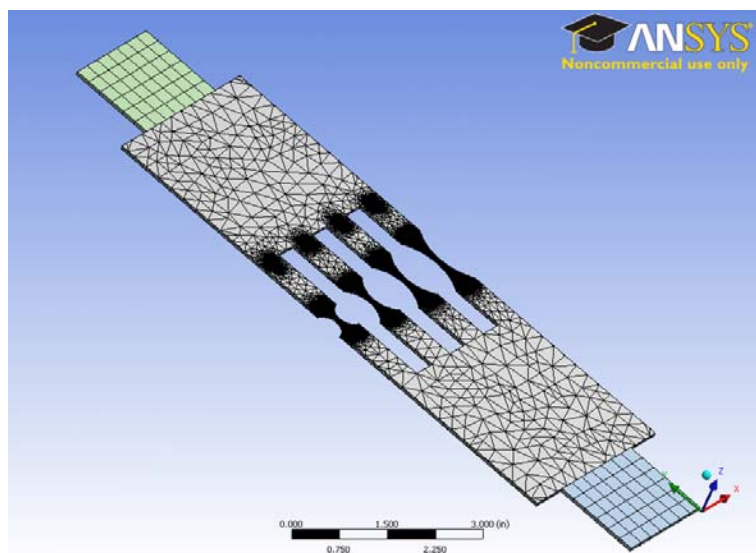


Figure 6: ANSYS Mesh for TFTS Model

Table 1: Finite Element Mesh Parameters for TFTS

FE Mesh	TFTS
Nodes	123,686
Elements	72,827

Model simulations were run for the 0.51 mm (0.02 inch) and 0.25 mm (0.01 inch) displacement conditions representing the limits of the experimental controls. Table 2 summarizes the finite element results. These nominal stress values were used in the MATLAB fatigue life estimation code.

Table 2: Nominal Stresses Found from ANSYS TFTS Model, MPa (psi)

Notch Radius mm (in)	Nominal Stresses, MPa (psi)	
	0.5 mm (0.02 in) disp. (S1)	0.2 mm (0.01 in) disp. (S2)
6.4 (0.25)	150.2 (21,795)	75.1 (10,898)
12.7 (0.5)	141.4 (20,517)	70.7 (10,259)
19.0 (0.75)	129.7 (18,817)	64.7 (9,408)
25.4 (1.0)	122.0 (17,702)	61.0 (8,851)

A representative *y*-direction (axial) component stress plot from the ANSYS TFTS model is in Figure 7.

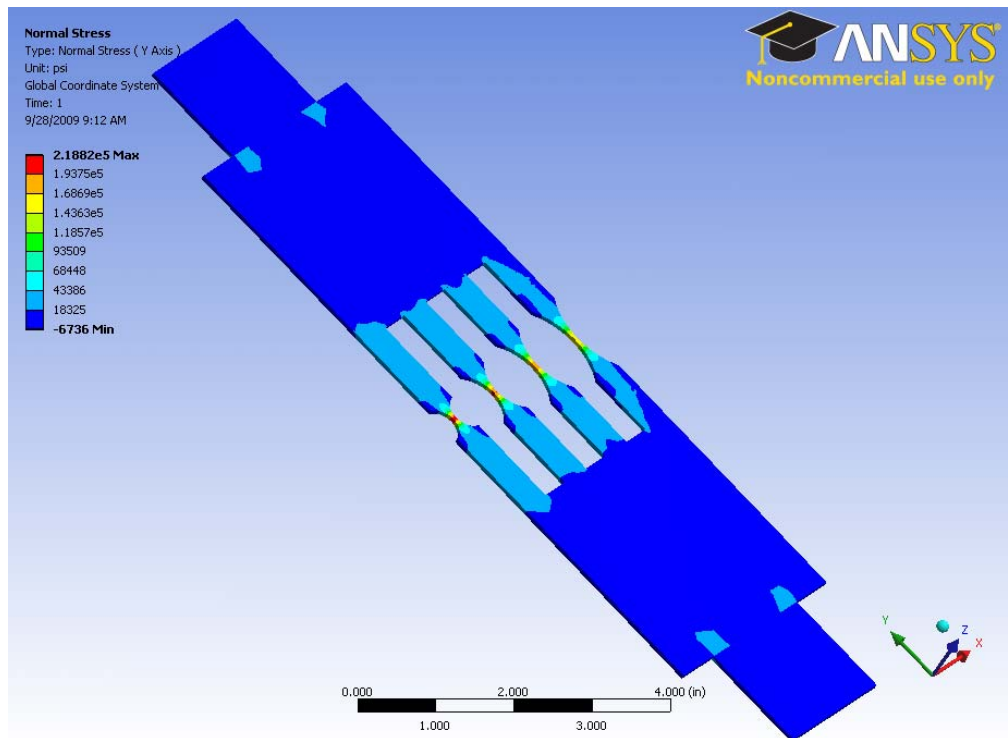


Figure 7: ANSYS TFTS Model; Y-Axis Normal Stress

4.1.3 Sensor Fatigue Life Estimates

The required input parameters for the life estimation code were the strain-life fatigue parameters for the 7075-T6 aluminum sensors, the notch stress concentration factors K_{tg} , and the nominal stresses obtained from the finite element studies (Table 2). The strain-life parameters were derived from 7075-T6 experimental data produced by Endo and Morrow [12]. The material properties along with the strain-life parameters of 7075-T6 aluminum can be seen in Table 3 below.

Table 3: Sensor Material Properties [12, 11]

Monotonic Material Properties	7075 T6 Alum
Modulus of Elasticity (E), ksi	10,300
Yield Strength (Sy), ksi	68
Ultimate Strength (Su), ksi	84
Reduction of Area, %	33
Poisson Ratio	0.33

Strain-Life Properties	7075 T6 Alum
fatigue strength coefficient, ksi	128.75
fatigue strength exponent	-0.0762
fatigue ductility coefficient	0.4664
fatigue ductility exponent	-0.7779
cyclic strain hardening exponent	0.097956
cyclic strength coefficient, ksi	138.738

These strain-life parameters were derived [11] from the experimental data from Endo and Morrow's cyclic testing of 7075-T6 [12].

The stress concentration factor input parameter was found using the data for shallow U-shaped notches given in Peterson [13], Figure 8.

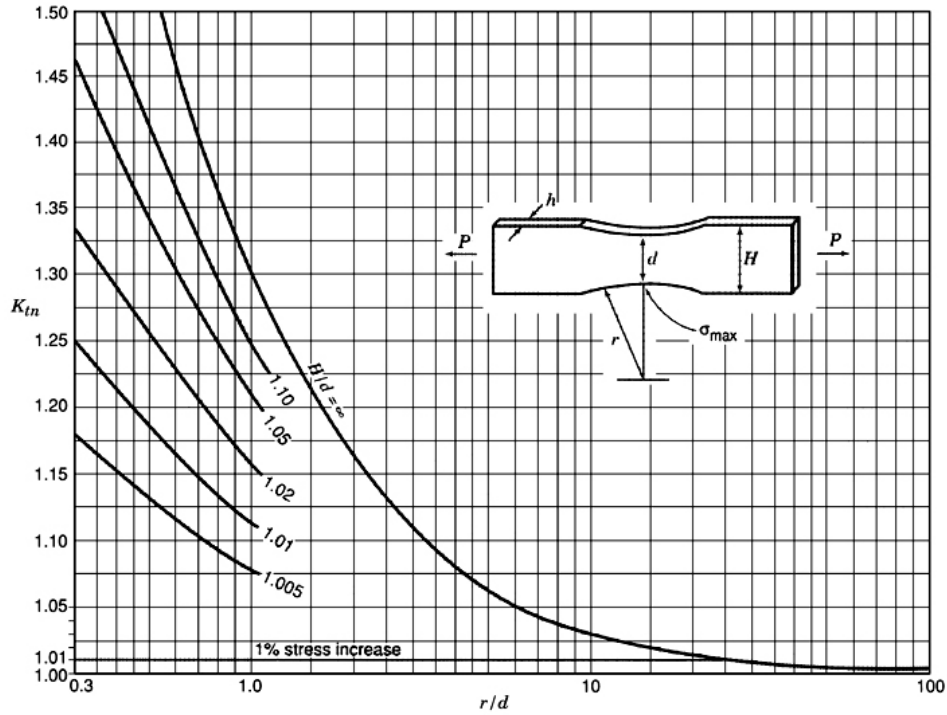


Figure 8: Stress Concentration Factors for Shallow U-shaped Notches [13]

The H/d parameter in Figure 8 is assumed to be ∞ in this case because of the TFTS geometry. The nominal stresses found in the ANSYS TFTS model are expressed in terms of the gross area K_{tg} whereas Figure 7 gives a stress concentration factor K_{tn} based on the net area. K_{tn} is converted to K_{tg} by

$$K_{tg} = \frac{H}{d} K_{tn}$$

where H is the arm gross section width (i.e., without the notch), d is the arm net section width, and h is the thickness. For the four sensor arm radii studied here, the estimated stress concentration factors are summarized in Table 4.

Table 4: Tensile Fatigue Test Specimen Stress Concentration Factors

Stress Concentration Factor	TFTS Sensor Arm Notch Radius			
	6.4 mm (0.25 in)	12.7 mm (0.50 in)	19.0 mm (0.75 in)	25.4 mm (1.0 in)
K_{in}	1.0625	1.03	1.02	1.015
K_{tg}	9.5625	9.27	9.18	9.135

As a point of comparison, the stress concentrations computed from the finite element results are summarized in Table 5 for both the maximum and minimum displacement conditions; in Table 6 the computed values are compared to the handbook values.

Table 5: ANSYS Calculated Tensile Fatigue Test Specimen Stress Concentration Factors

0.51 mm (0.02 in) Displacement			
Notch radius mm (in)	Max Stress MPa (psi)	Nominal Stress	
		MPa (psi)	K_{tg}
6.4 (0.25)	1,508 (218,820)	149.6 (21,696)	10.09
12.7 (0.5)	1,408 (204,290)	141.4 (20,503)	9.96
19.0 (0.75)	1,291 (187,200)	130.5 (18,931)	9.89
25.4 (1.0)	1,172 (169,940)	122.4 (17,762)	9.57
0.25 mm (0.01 in) Displacement			
Notch radius mm (in)	Max Stress MPa (psi)	Nominal Stress	
		MPa (psi)	K_{tg}
6.4 (0.25)	754.3 (109,410)	74.8 (10,848)	10.09
12.7 (0.5)	703.6 (102,060)	70.7 (10,251)	9.96
19.0 (0.75)	644.9 (93,542)	65.2 (9,465)	9.88
25.4 (1.0)	586.0 (85,000)	61.2 (8,881)	9.57

The stress concentration values found from the ANSYS TFTS model listed in the table above are compared to the handbook values in Table 6. Clearly the stress concentration values for the ANSYS model and the values based off of the chart are within reasonable agreement of each other indicating that the ANSYS model is providing good results and can be used in further simulations.

Table 6: Stress Concentration Factors Found from ANSYS and K_t Chart

Notch radius mm (in)	TFTS K_{tg}	
	ANSYS	Chart
6.4 (0.25)	10.09	9.56
12.7 (0.5)	9.96	9.27
19.0 (0.75)	9.88	9.18
25.4 (1.0)	9.57	9.14

4.1.4 Comparison of Theory and Experiment

Based upon the input parameters discussed above, the number of cycles to failure for the sensor arms were estimated using the Morrow mean stress, Manson-Halford mean stress, and Smith-Watson-Topper mean stress criteria, given by [14]

Morrow:

$$\frac{\Delta\varepsilon}{2} = \frac{\sigma'_f - \sigma_0}{E} (2N_f)^b + \varepsilon'_f (2N_f)^c$$

Manson-Halford:

$$\frac{\Delta\varepsilon}{2} = \frac{\sigma'_f - \sigma_0}{E} (2N_f)^b + \varepsilon'_f \left(\frac{\sigma'_f - \sigma_0}{\sigma'_f} \right)^{c/b} (2N_f)^c$$

Smith-Watson-Topper:

$$\left(\frac{\Delta\sigma}{2} + \sigma_0 \right) \frac{\Delta\varepsilon}{2} = \frac{(\sigma'_f)^2}{E} (2N_f)^{2b} + \sigma'_f \varepsilon'_f (2N_f)^{b+c}$$

Each of these models approaches the non-zero mean stress case differently and we want to compare their relative performance.

A total of eight TFTS specimens were cycled to failure in the MTS machine under a maximum and minimum displacement condition of 0.02 and 0.01 inches, respectively. The number of cycles to failure was captured manually for each of the notched arms present in the tensile fatigue test specimens. When a notched arm failed, it produced a high pitch ringing noise and the cycle number was captured at that point in time. Table 7 below gives the results for the eight tests.

Table 7: Tensile Fatigue Test Specimen Experimental Results

Notch Size, rad. mm (in)	Cycles to Failure							
	Test 2	Test 3**	Test 4*	Test 6*	Test 8*	Test 9**	Test 10	Test 11*
6.4 (0.25)	2,630	3,125	1,857	1,888	2,938	2,977	930	2,341
12.7 (0.5)	3,065	2,136	1,857	1,888	2,938	2,571	2,334	2,341
19.0 (0.75)	3,926	4,868	4,975	4,079	6,034	3,197	3,674	4,445
25.4 (1.0)	8,714	8,114	8,610	5,730	9,208	5,948	6,374	9,757

** the second smallest notch (12.7 mm; 0.50 inch) broke first

* the smallest (6.4 mm; 0.25 inch) and the second smallest (12.7 mm; 0.50 inch) broke at the same time.

The TFTS model simulation produced the following theoretical results based on cycles to failure.

Table 8: Tensile Fatigue Test Specimen Theoretical Model Simulation Results

Notch Radius mm (in)	Strain-Life Criteria, Cycles to Failure		
	Morrow	M-H	SWT
6.4 (0.25)	1,709	183	2,012
12.7 (0.5)	2,494	397	3,456
19.0 (0.75)	3,944	961	6,427
25.4 (1.0)	5,682	1,839	10,141

A graphical comparison between the theoretical results and the experimental results can be seen in Figures 9-11 below. The graphs show the cycles to failure for each notch radius r .

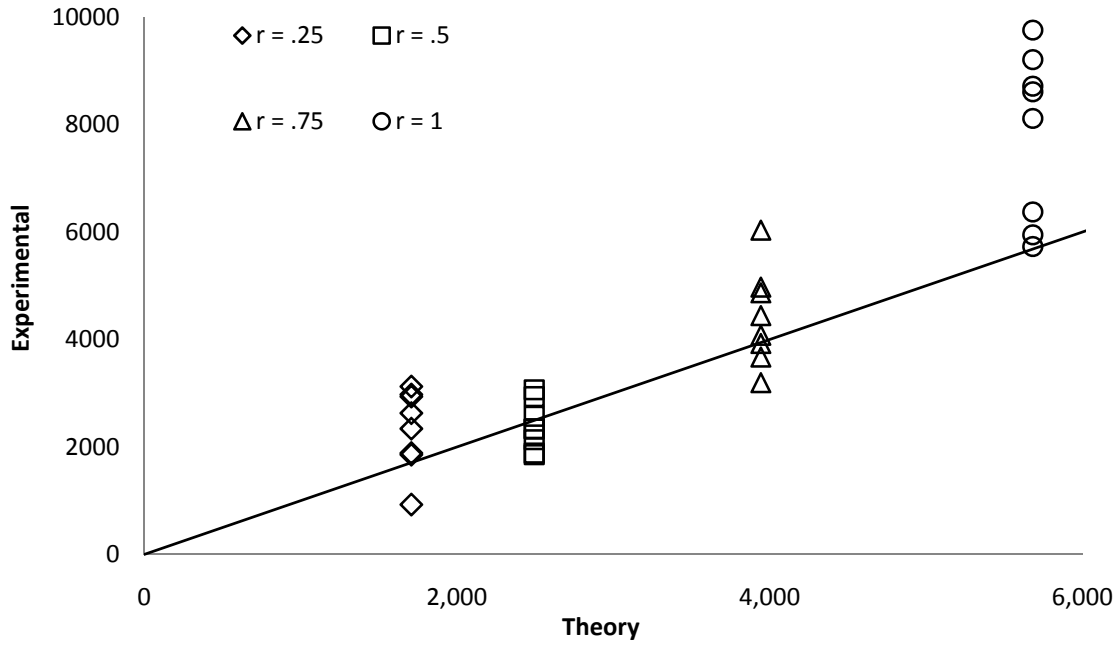


Figure 9: Experimental vs. Theoretical Life - Morrow Criterion

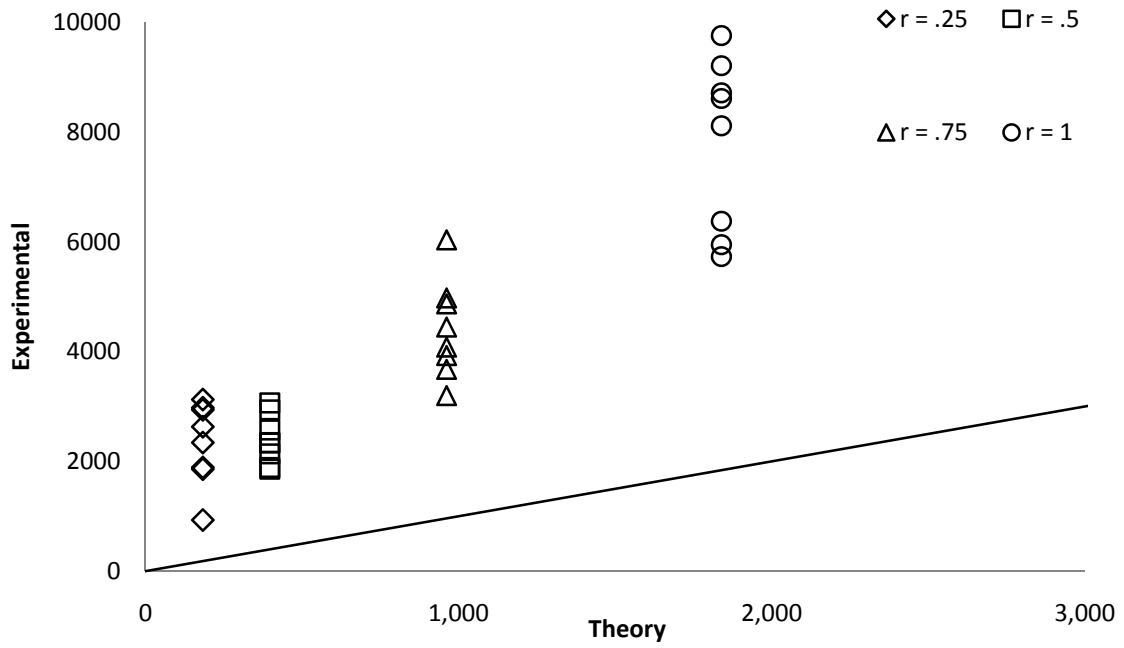


Figure 10: Experimental vs. Theoretical Life - M-H Criterion

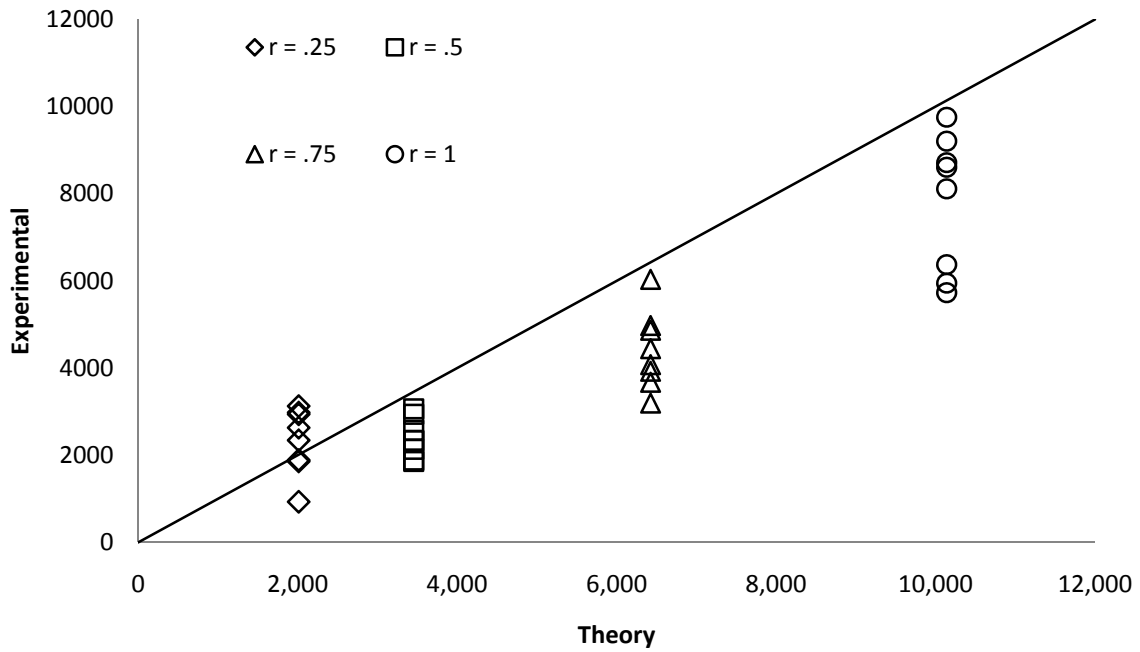


Figure 11: Experimental vs. Theoretical Life - SWT Criterion

It can be seen from these Figures that the Morrow and SWT strain-life theories model the experimental results better than the M-H theory. We see that the Morrow criterion tends to under predict the experimental results while the SWT criterion tends to over predict. These trends tend to show themselves most prominently at the higher notch radii. While conducting the TFTS experiments, we noted that progressive sequential failure (smallest to largest notch radius) only occurred twice out of the eight tests. Out of the other six tests, either the smallest ($r = 6.4$ mm [0.25inch]) and second smallest ($r = 12.7$ mm [0.5 inch]) notch failed at the same time, or the second smallest ($r = 12.7$ mm [0.5 inch]) notch failed first, then the smallest ($r = 6.4$ mm [0.25]) notch failed, while the larger notches failed in order. The reasoning for the notches failing out of sequential order from smallest to largest could possibly be explained by the stress concentrations of the notches. When looking at Table 6, it can be seen that the stress concentration factors were all very close to one another. This is further reflected in Table 5 where we found that the nominal stresses of the smallest and second smallest notches are close to one another. This indicates that the load passing through these notches is almost the same and this could possibly explain the failure of the smallest and second smallest notch at the same exact time as well as the failure of the second smallest notch before the smallest notch.

Overall the tensile fatigue test results showed that successive failures can be accomplished in specimens with notch geometries undergoing tensile loading in the MTS machine. Creating notch geometries with stress concentration factors close to one another can create problems with progressive sequential failure. Using notched armed geometries with greater differences in stress concentration factors can mitigate the problems of notches not failing in the correct order of stress concentration magnitude because of the stress concentration factors being so close to one another.

4.2 PROTOTYPE FATIGUE SENSOR PERFORMANCE

The information gathered from the proof-of-concept TFTS guided our development of the prototype fatigue sensor that was designed for bonding to an underlying structure experiencing constant amplitude cyclic loading scenarios. The goal of this phase of testing was to gain an understanding of the behavior of the fatigue sensor (FS) attached to the carrier specimen (CS) as the CS underwent cyclic loading. The FS design consisted of three different notched armed geometries. Given our experience with the shallow notches in the TFTS, we chose to use a more aggressive notch geometry in these sensors and adopted a deep U-notch design. The concept behind this FS was that the cyclic strain being experienced by the CS would be transferred to the FS, and the FS would experience progressive sequential failure of each of its notched armed geometries due to the local stress concentrations present in the arms. The materials used in this experiment were 1018 steel (220.6 MPa [32 ksi] yield strength) for the carrier specimen and 7075-T6 aluminum (Table 3) for the fatigue sensor.

4.2.1 Deep U-Notch Sensor Design and Testing

The FS was designed in 3-D CAD software for ease of manufacturing, and the two FS designs used in the experiments were designated as types 2A and 1B. The 2A FS design holds the notch ligament width constant while varying each of the three notch radii. The 1B FS design does

exactly the opposite, holding the notch radius constant while varying each of the three ligament widths. These two prototype sensor designs are shown in Figures 12 and 13.

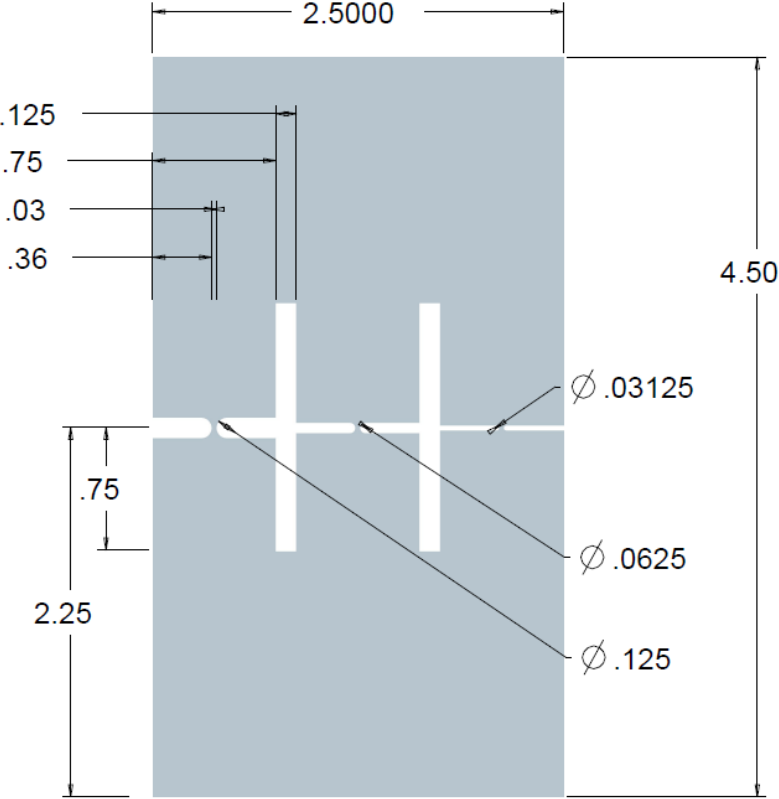


Figure 12: Fatigue Sensor Type 2A Geometry [All Dimensions in Inches]

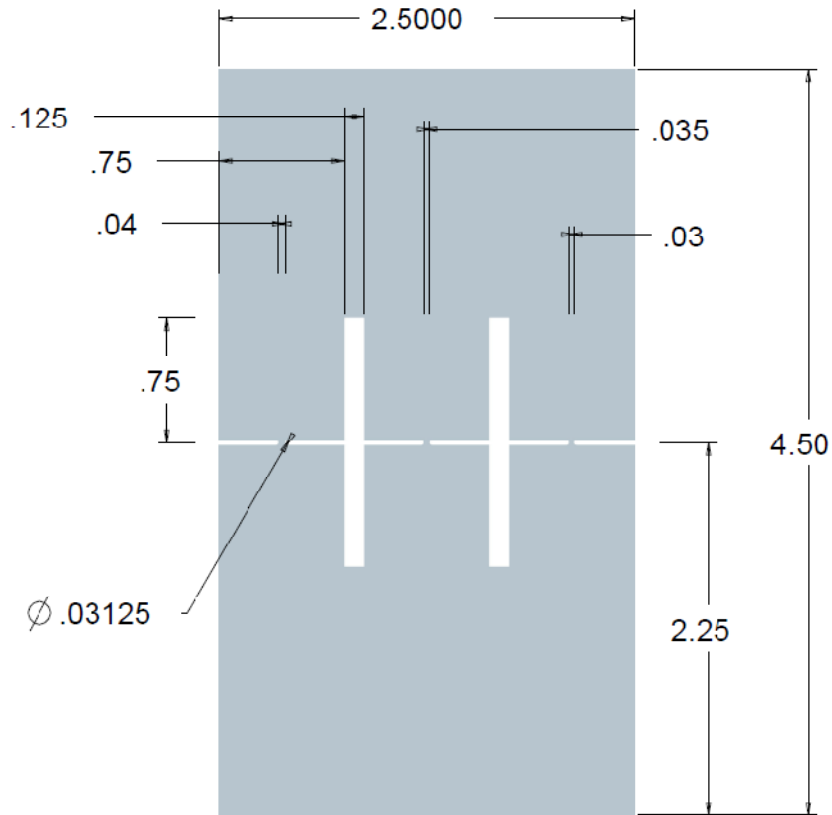


Figure 13: Fatigue Sensor Type 1B Geometry [All Dimensions in Inches]

The FS were CNC machined from 7075-T6 sheets of aluminum with a thickness of 0.81 mm (0.032 inch). The carrier specimens (CS) were made from 1018 hot rolled 3.2 mm (0.125 inch) thick steel sheet and were cut to dimensions 381 × 76.2 mm (15 × 3 inch). Spacers separating the FS from the CS were cut from 7075-T6 sheets of aluminum with size of 25.4 × 63.5 × 1.6 mm (1 × 2.5 × 0.063 inch).

The test specimens were comprised of a CS, a FS, and two spacers each. The FS and spacers were cleaned with a degreaser and the surface of the CS, to which the FS would be adhered to, was sanded and cleaned to remove any dirt or rust build up. Next the FS, CS, and spacers were abraded with medium grade sand paper and cleaned again. This was done to create a rough surface for the adhesive to bond to. When the preparation procedures were completed the FS, CS, and two spacers were glued together using 3M brand DP810 Acrylic Adhesive. Once all the test specimen parts were glued together, the test specimens were allowed to sit for at least 72 hours to assure complete adhesive curing.

The tensile FS tests were performed using the MTS servohydraulic testing machine, Figure 14. The tests were run under sine wave force control at a frequency of 1 Hertz. The test specimens were gripped in the MTS machine 38.1 mm (1.5 inch) from the top and the bottom. A bubble level was used each time a test specimen was gripped to ensure the test specimen was as close to vertical as possible.



Figure 14: Close Up of Mounted Fatigue Sensor

Once the test specimen was gripped in the MTS machine, the load cell was zeroed so that no preload existed on the specimen. A series of nine experiments were carried out for each of the two FS geometries. Three different loads were tested with three tests per loading condition. The tests were carried out under a stress ratio ($\sigma_{\min}/\sigma_{\max}$) of 0.05 and the maximum loads used were a percentage of 220.6 MPa (32 ksi) yield strength, S_y , of the 1018 HR steel CS material. Table 9 below summarizes the three loading conditions.

Table 9: Test Loading Conditions

% of S_y	Axial load kN (lbs)	
	max	min
80	42.7 (9,600)	2.1 (480)
70	37.4 (8,400)	1.9 (420)
60	32.0 (7,200)	1.6 (360)

The number of cycles to failure for each FS arm was captured manually. At 80 and 70 percent of yield loading conditions the notched arm geometries would make a distinct sound when failure of the notched arm occurred. As soon as the distinct sound of a notched arm failing was heard

the cycle number was recorded and then the notched arm was examined with a magnifier to confirm that the notched arm had failed. At 60 percent of yield there was no distinct sound when a notched arm had failed. These specimens were monitored using an optical magnifier, observing the cracking progress through fracture. The cycle number was then recorded when complete separation could be seen.

4.2.2 Fatigue Sensor Model Simulation

As before, we constructed finite element models to predict the behavior of the prototype fatigue sensors and obtain comparison data for the experiments. In this case, however, the presence of the CS complicated the determination of the appropriate loads to apply to the sensor model. A test specimen comprised of a dummy FS, CS, and two spacers (Figure 15) was fabricated for strain data collection. The dummy FS geometry was a $114 \times 63.5 \times 0.81$ mm ($4.5 \times 2.5 \times 0.032$ inch) piece of 7075-T6 aluminum just like the FS used in the experimental tests, but without the notched arms present. The dummy FS and CS were outfitted with foil strain gages on both the front and back surfaces, placed as close as possible to the center locations of the CS and dummy FS.

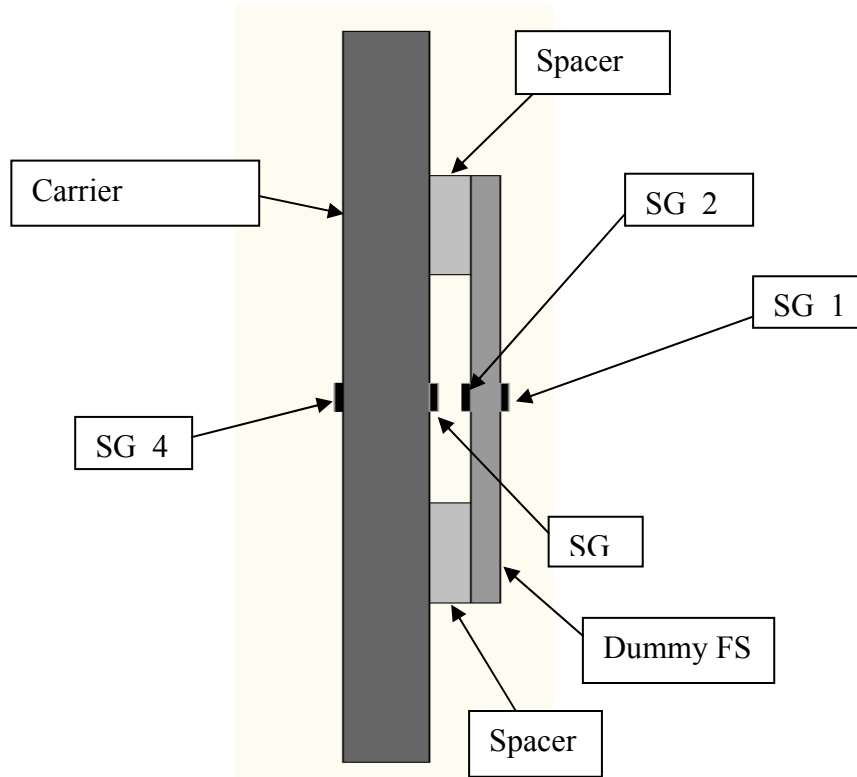


Figure 15: Dummy Fatigue Sensor Test Specimen Schematic

After fabrication of this specimen, the strain gages were wired into a National Instruments data acquisition system consisting of a SC-2345 signal conditioning chassis, SCC-SG01 quarter bridge signal conditioners, and a 6062E DAQ card. National Instruments' LabVIEW version 8.5 was the data acquisition software. The strain gage modules were zeroed as closely as possible with a fluctuation of about ± 75 micro strain present in each of the strain gage reading outputs.

The loading conditions for the dummy FS tests were the same as those to be used in the prototype FS testing, as shown in Table 9. The averaged measured strains for the three different loading conditions were recorded and converted to displacements by the relation

$$\varepsilon = \frac{\Delta L}{L}$$

where L is 63.5 mm (2.5 inch) and ε is the measured peak strain value. Table 10 below summarizes the averaged measured peak strains along with the corresponding calculated displacement values for the loading conditions considered.

Table 10: Measured Peak Strains and Calculated Displacements

% of Sy	Average Measured Strain	
	SG 1	SG 2
80	0.0006717	0.0006138
70	0.0005962	0.0005421
60	0.0005122	0.0004653
% of Sy	Calculated Displacement mm (in)	
	SG 1	SG 2
80	0.042 (0.0016793)	0.039 (0.0015345)
70	0.038 (0.0014905)	0.034 (0.0013553)
60	0.032 (0.0012805)	0.030 (0.0011633)

The calculated displacement values found from the dummy FS test specimen were used in a finite element analysis to find the nominal stresses present in the notched arms of the FS; the CS and two spacers were not used in the model simulation. ANSYS Workbench was used the analysis. The FS model in ANSYS was partitioned into three sections, a lower and upper tab and a central section with the notched sensor arms. Each of the sections in the model was given 7075-T6 aluminum material properties. The finite element meshes used in the ANSYS FS models were refined in the presence of the notches are shown in Figures 16 and 17, and the mesh statistics are summarized in Table 11.

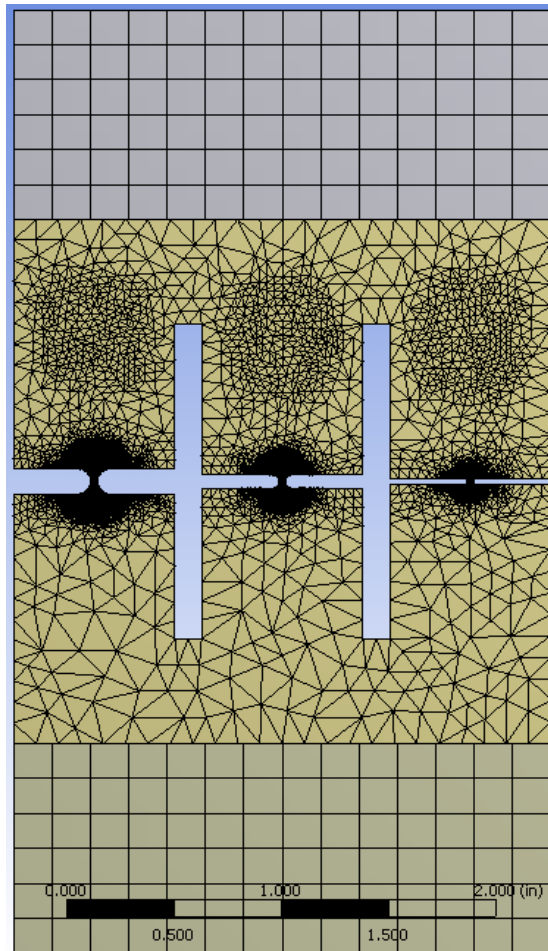


Figure 16: ANSYS Mesh for 2A FS Geometry

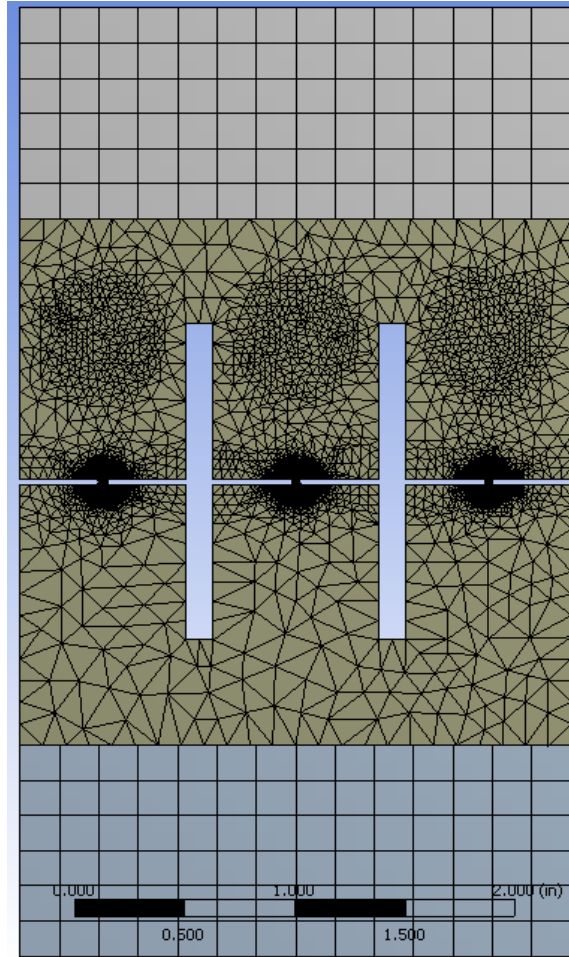


Figure 17: ANSYS Mesh for 1B FS Geometry

Table 11: Finite Element Mesh Parameters for ANSYS FS Model

FE Mesh	Fatigue Sensor	
	2A	1B
Nodes	172,919	136,418
Elements	105,946	83,004

The boundary conditions used in the ANSYS FS models were chosen to mimic the behavior of the real FS test specimen. In the real FS test specimen, the strain experienced by the FS is induced through displacements. In the ANSYS FS model, the upper tab was given a fixed support boundary condition and the displacement was applied to the lower tab. Frictionless supports were applied to the outer surfaces of the middle section removing any perpendicular

displacement perpendicular. Both of the ANSYS FS models 2A and 1B employed the same boundary conditions.

The nominal stress results from the finite element studies based on the experimental SG1 and SG2 results are summarized in Table 12 below. These are the stresses that were computed in the three notched arms, remote from the notches, and thus out of the notch-induced stress gradients. The locations of these nominal stresses were the same in the 2A and 1B geometries.

Table 12: Nominal Stresses Found from ANSYS FS Model MPa (psi)

2A FS Geometry						
% of Sy	Upper limit (SG 1)			Lower limit (SG 2)		
	1.59 mm (1/16 in)	0.79 (1/32)	0.40 (1/64)	1.59 (1/16)	0.79 (1/32)	0.40 (1/64)
60	15.5 (2,250)	16.4 (2,380)	17.5 (2,538)	14.1 (2,044)	14.9 (2,162)	15.9 (2,306)
70	18.0 (2,619)	19.1 (2,771)	20.4 (2,954)	16.4 (2,382)	17.4 (2,519)	18.5 (2,686)
80	20.3 (2,951)	21.5 (3,121)	22.9 (3,328)	18.6 (2,697)	19.7 (2,854)	21.0 (3,042)

1B FS Geometry						
% of Sy	Upper limit (SG 1)			Lower limit (SG 2)		
	1.01 mm (0.04in)	0.89 (0.035)	0.76 (0.03)	1.01 (0.04)	0.89 (0.035)	0.76 (0.03)
60	18.7 (2,717)	17.8 (2,587)	17.5 (2,543)	17.0 (2,468)	16.2 (2,350)	15.9 (2,310)
70	21.8 (3,163)	20.8 (3,012)	20.4 (2,959)	19.8 (2,876)	18.9 (2,738)	18.6 (2,691)
80	24.6 (3,563)	23.4 (3,393)	23.0 (3,334)	22.4 (3,256)	21.4 (3,101)	21.0 (3,047)

A representative stress contour plot from one of the ANSYS FS model simulations is given in Figure 18 below. The smooth stress contours are as expected and reveal the very large stress increase in the notch over the nominal (remote) value.

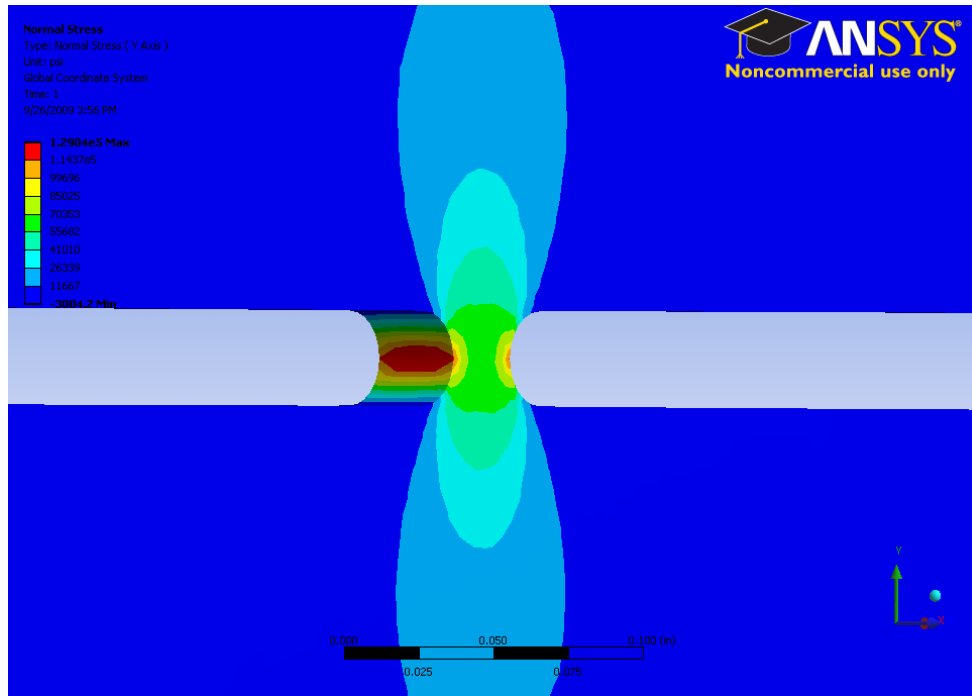


Figure 18: ANSYS 2A FS Model Y-Axis Normal Stress Close up 0.40 mm (1/64 inch) Notch

Once the nominal stresses were found from the ANSYS FS models, they became input parameters into the MATLAB fatigue code to calculate the number of cycles to failure for each of the notch geometries. The input parameters for the MATLAB code were the strain-life fatigue parameters for the material being analyzed, the nominal stress values S1 (maximum) and S2 (minimum), and the stress concentration factor K_{tg} . As before, the Morrow mean stress, Manson and Halford mean stress, and Smith Watson Topper mean stress criteria were used to estimate the fatigue life of the notches.

For the deep U-shaped notches, the stress concentration factors input parameter were found using Peterson [13]. The stress concentration charts, Figures 19 and 20 below, were used to determine the stress concentration factor input parameters for the 2A and 1B FS geometries.

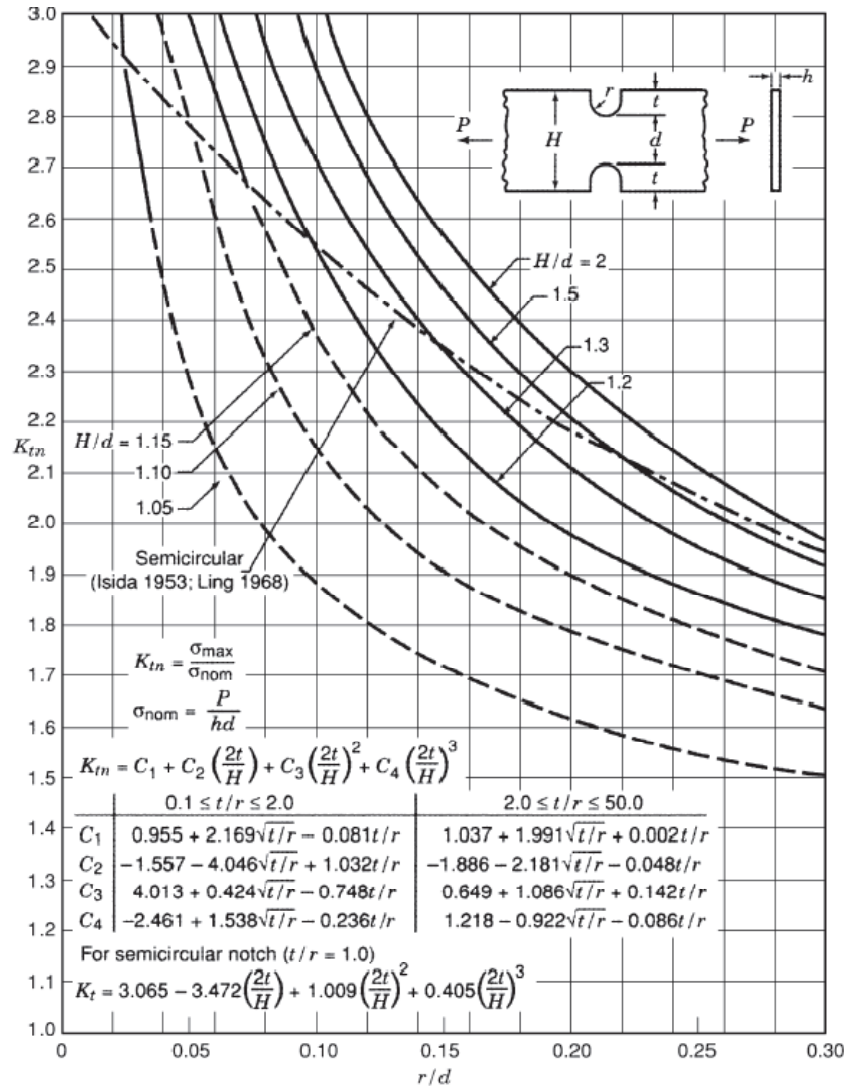


Figure 19: Stress Concentration Chart for Opposed U-Shaped Notches [13]

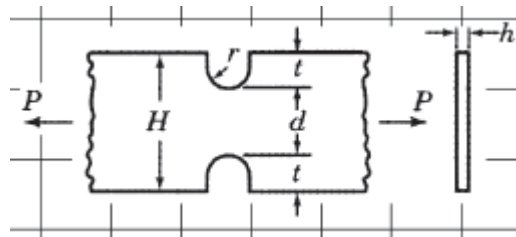


Figure 20: Geometry Basis for Opposite U-Shaped Notches [13]

For the three notch sizes used in each FS specimen type, the geometric definition is summarized in Table 13. It can be in Table 13 that the H/d parameters for the 2A and 1B FS geometries are too large to use the plotted curves in the stress concentration chart (Figure 19), so the curve fit polynomial equation was utilized instead in determining the stress concentration factors. The computed SCF's are summarized in Table 14.

Table 13: U-Shaped Notch Geometry Parameters for 2A and 1B FS

geometry parameters	2A FS Geometry			1B FS geometry		
	1.59 mm (1/16 in)	0.79 mm (1/32 in)	0.40 mm (1/64 in)	1.0 mm (0.04 in)	0.89 mm (0.035 in)	0.76 mm (0.03 in)
t/r	5.76	11.52	23.04	22.72	22.88	23.04
H/d	25	25	25	18.75	21.43	25

Table 14: Fatigue Sensor Stress Concentration Factors

Stress Conc. Factor	2A FS Geometry			1B FS geometry		
	1.59 mm (1/16 in)	0.79 mm (1/32 in)	0.40 mm (1/64 in)	1.0 mm (0.04 in)	0.89 mm (0.035 in)	0.76 mm (0.03 in)
K_{tn}	1.16	1.31	1.55	1.68	1.61	1.55
K_{tg}	29.09	32.71	38.72	31.45	34.57	38.72

Using the curve fit polynomial equation gives the net section stress concentration factor K_{tn} . The theoretical stress concentration factor K_{tg} is based on the gross area and was found using relationship between the two noted above.

4.2.3 Comparison of Results

The experimental results from the tensile FS tests based off of the 2A and 1B FS designs can be seen in the tables below. For each loading condition there is three data points for each of the notch geometries present in the FS.

Table 15: Model 2A Experimental Cycles to Failure

Loading Condition	# of Cycles to Failure		
	0.79 mm (1/32 in)	1.59 mm (1/16 in)	3.18 mm (1/8 in)
80% Sy	2,024	3,281	13,714
	2,961	4,489	10,158
	2,353	3,995	8,943
70% Sy	4,969	5,965	15,617
	6,557	10,768	14,066
	6,771	9,370	22,023
60% Sy	6,514	12,879	20,689
	9,704	11,893	18,150
	6,983	12,702	18,242

Table 16: Model 1B Experimental Cycles to Failure

Loading Condition	# of Cycles to Failure		
	0.76 mm (0.03 in)	0.89 mm (0.035 in)	1.02 mm (0.04 in)
80% Sy	2,439	2,824	5,174
	2,053	2,746	4,124
	2,269	3,350	5,344
70% Sy	4,342	6,263	9,101
	4,001	5,261	5,458
	5,015	5,926	8,169
60% Sy	7,204	9,345	15,064
	6,503	9,633	12,037
	9,766	11,018	13,117

There were a total of six finite element-based simulations performed for each of the FS designs. For each of the three percentage of yield loading conditions, there were two simulations performed, one based on the displacement data calculated from the SG 1 strain gage results and the other based on the SG 2 strain gage results. The SG1 strain gage produced higher calculated displacements due to the fact that it was mounted on the concave side of the dummy FS. Higher displacements produce higher nominal stresses and higher nominal stresses produce a lower number of cycles to failure. The SG2 strain gage produced lower calculated displacements due to the fact that it was mounted to the convex side of the dummy FS. Lower displacements produce lower nominal stresses and lower nominal stresses produce a higher number of cycles to failure.

Combining the experimental data (Tables 15 and 16) with the life simulations driven by the finite element stresses, Figures 27-32 summarize the performance of the 2A and 1B fatigue sensor prototypes. On these figures, we have plotted the stress (as a percentage of yield stress in the

carrier specimen) against the number of constant amplitude load cycles to failure. The failure trajectories predicted by the aforementioned mean stress models (Morrow, Manson-Halford, Smith-Watson-Topper) using the SG1 and SG2 data are shown, as are the corresponding experimental data points. One figure is drawn for each of the six notch geometries used in the FS prototypes.

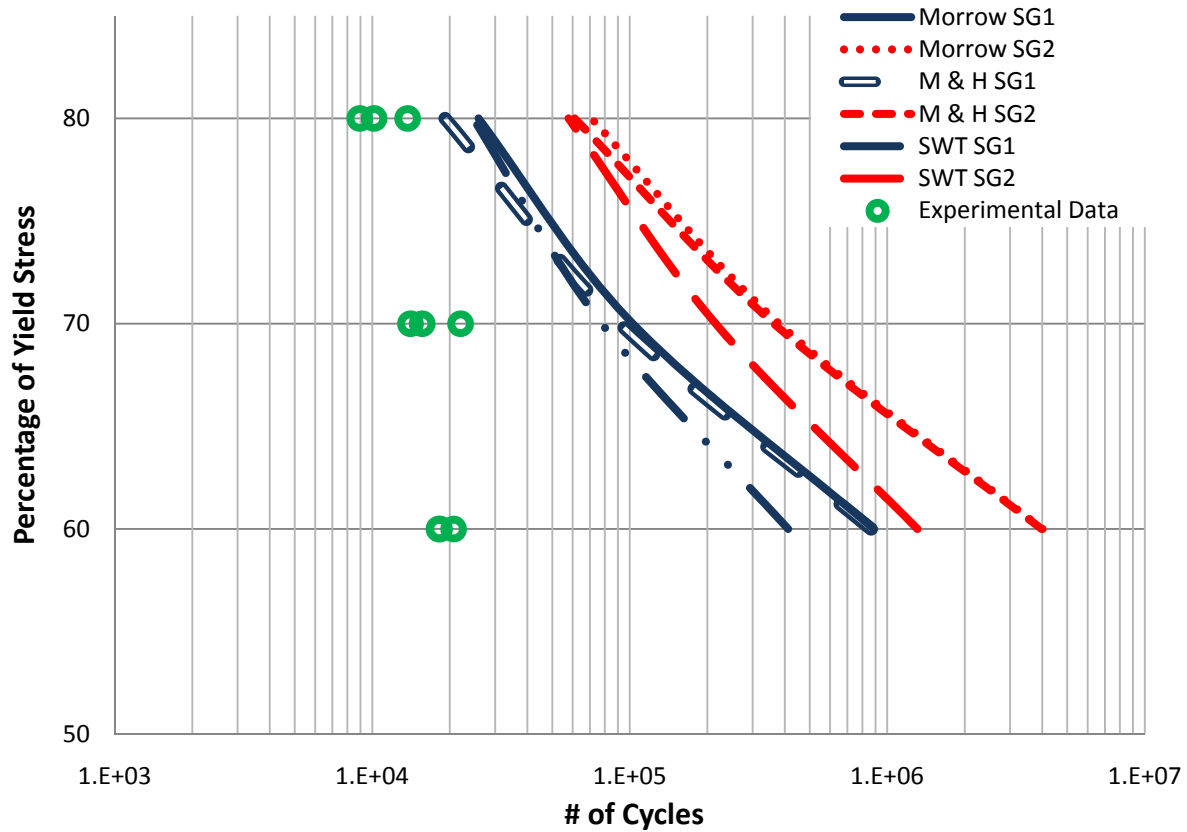


Figure 21: Fatigue Life of the 1.59 mm (1/16 inch) Notch Radius

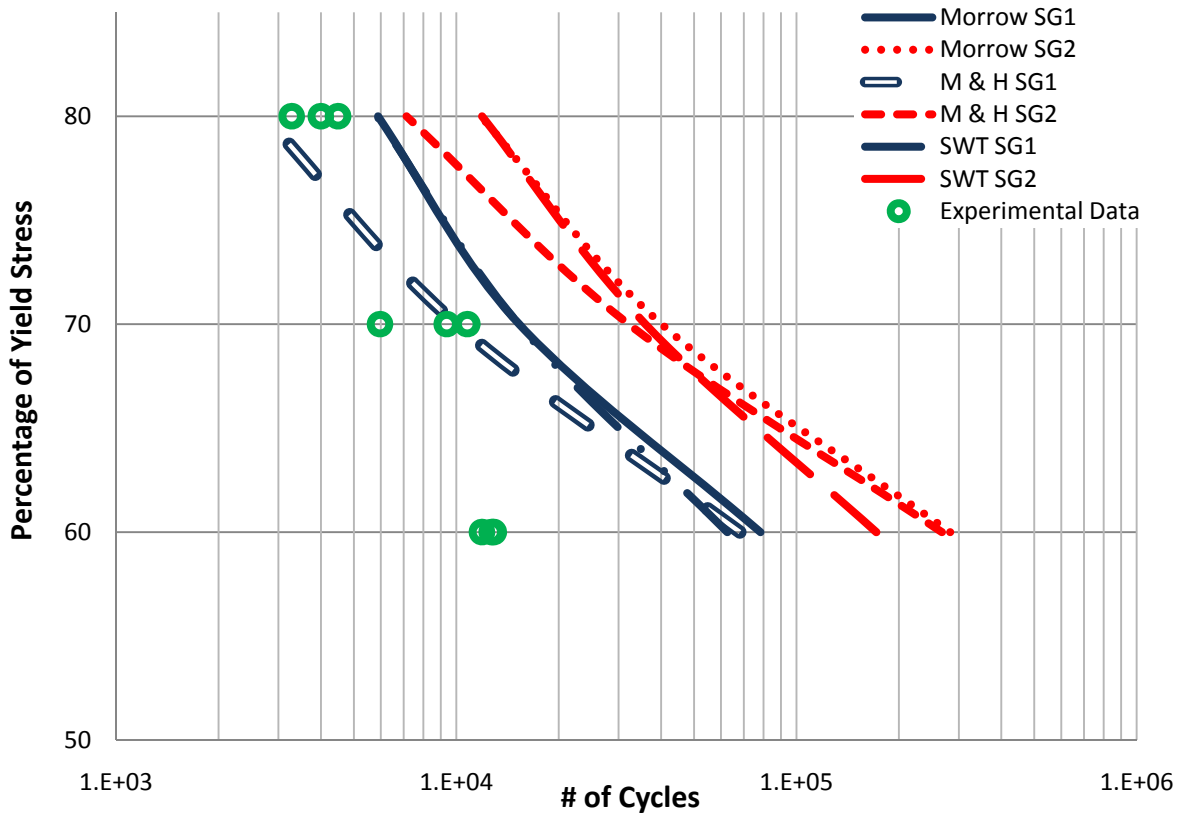


Figure 22: Fatigue Life of the 0.79 mm (1/32 inch) Notch Radius

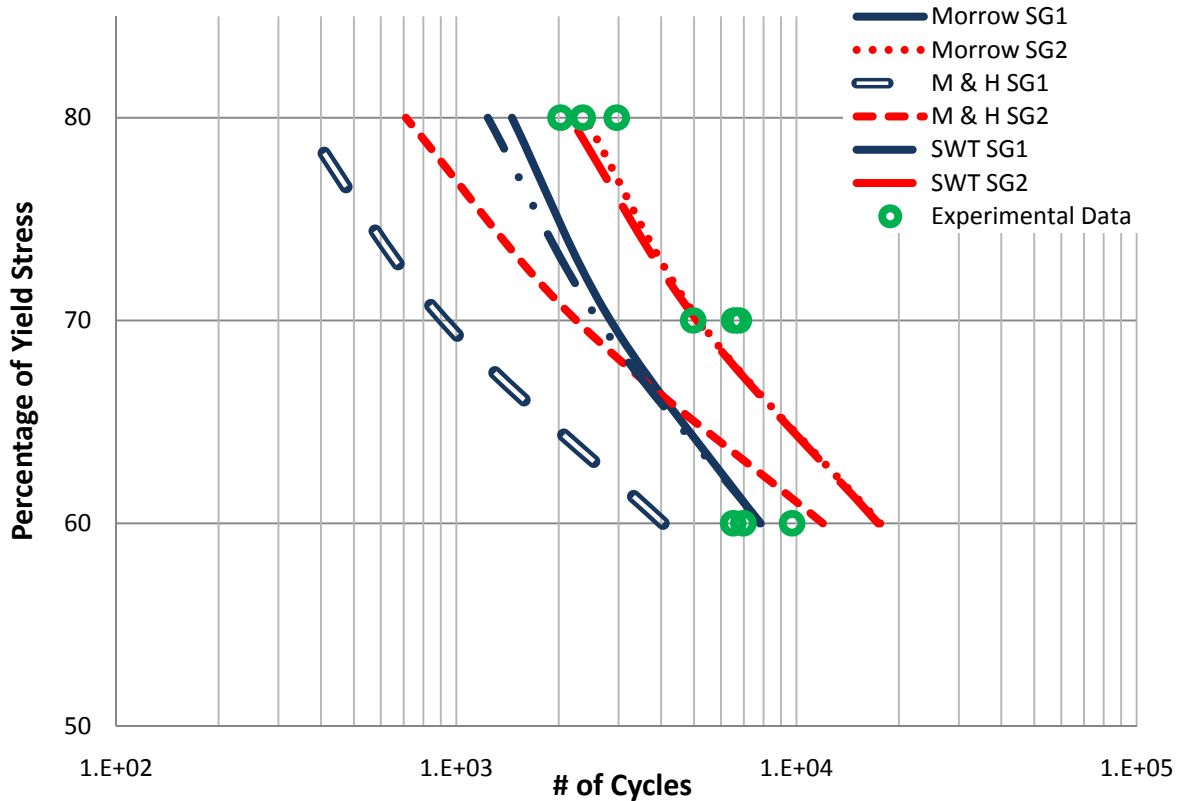


Figure 23: Fatigue Life of the 0.40 mm (1/64 inch) Notch Radius

Figures 21-23 above indicate that the 2A FS experimental data tends to agree more with the theoretical life curves as the notch radius decreases in size. In Figure 23, all the experimental data points are within or pretty close to the theoretical strain-life curves. The data points at the 80 and 70% yield loading conditions match up closer with the Morrow and SWT SG2 theoretical curves while the data points associated with the 60% yield loading condition match up closer with the Morrow SG1, SWT SG1, and M & H SG2 theoretical curves. In Figure 22, as the loading percentage of yield stress begins to decrease the experimental data points begin to deviate farther away to the left of the theoretical strain-life curves. At the 80% yield loading condition the data points fall within the Morrow, M & H, and SWT SG1 theoretical curves. At the 70% yield loading conditions the data points match up closest with the M & H SG1 theoretical curve. The data points at the 60% yield loading condition are pretty far from the theoretical curves when compared to the 80 and 70% yield loading conditions. In Figure 21, none of the data points fall within the bounds of the theoretical strain-life curves. The data points pertaining to the 80% yield loading condition are the closest to the theoretical curves and as the percentage of yield loading condition decreases the data points move farther away from the theoretical strain-life curves.

Combining the experimental and simulation results for the 1B FS design, we obtain Figures 24-26 below. As before, a variety of theoretical results are given for the varying ligament sizes characterizing the 1B geometry.

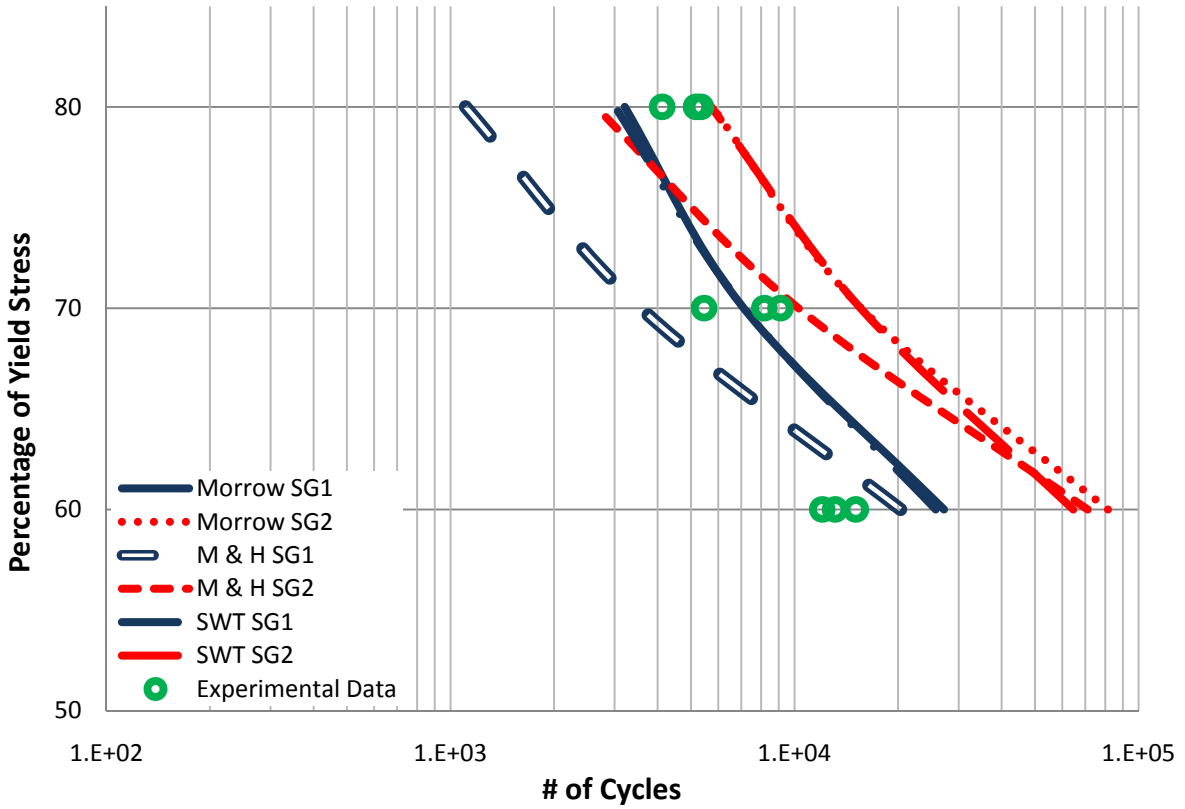


Figure 24: Fatigue Life of the 1.02 mm (0.04 inch) Notch Ligament

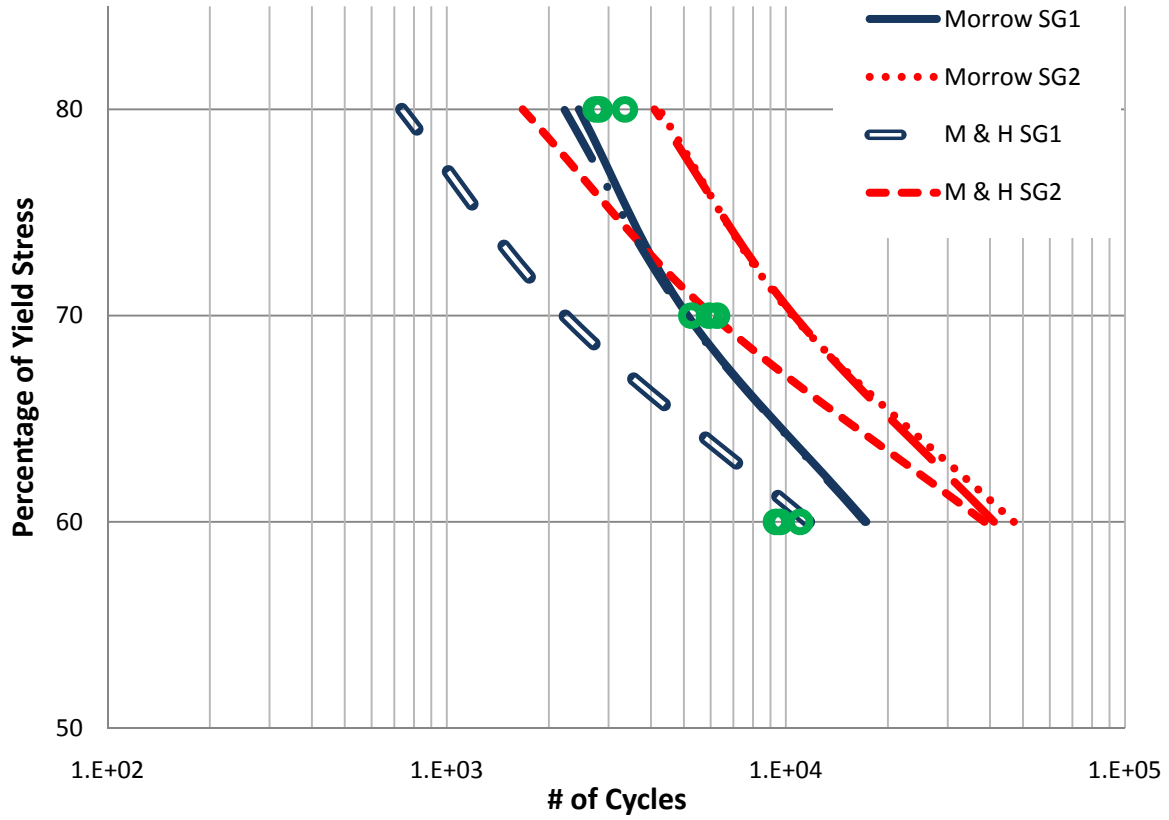


Figure 25: Fatigue Life of the 0.89 mm (0.035 inch) Notch Ligament

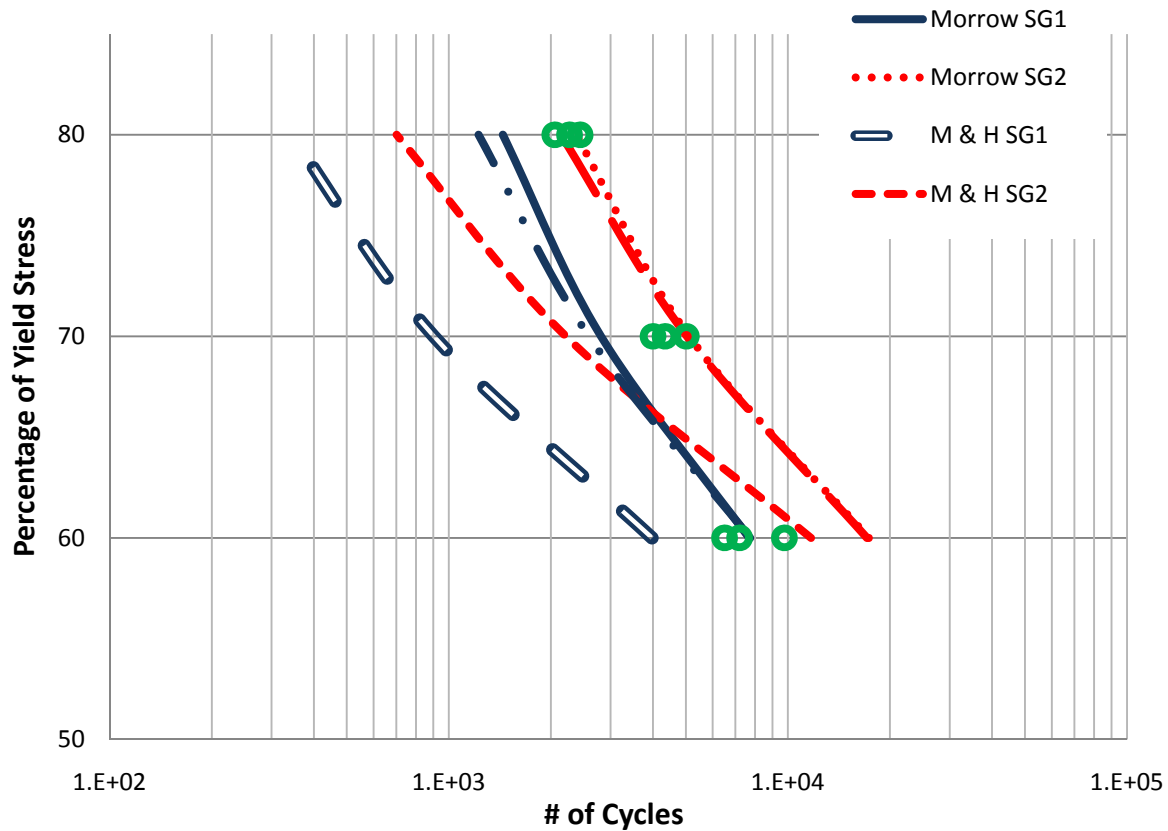


Figure 26: Fatigue Life of the 0.76 mm (0.03 inch) Notch Ligament

We see in Figures 24-26 above that the 1B FS experimental data is in good agreement with the theoretical life results for all ligament sizes in the series. In Figure 24, all the experimental data points except for the 60% yield loading condition fall within the bounds of the theoretical strain-life curves. The data points for the 60% yield loading condition fall just outside of the M & H SG1 theoretical strain-life curve. The data points corresponding to the 80% yield loading condition fall between the Morrow SG1, Morrow SG2, and SWT SG2 theoretical curves. The data points from the 70% yield loading condition match up closely with Morrow SG1, SWT SG1, and M-H SG2. The data points in Figure 25 are in almost identical locations of the data points in Figure 24. The 60% yield loading condition data points in Figure 27 come a little closer to the M-H SG1 theoretical strain-life curve when compared to the 60% yield data points in Figure 24. In Figure 26, all the experimental data points fall within the bounds of the theoretical strain-life curves. The data points from the 80% yield loading condition fall in line with Morrow SG2 and SWT SG2 theoretical strain-life curves. The data points corresponding to the 70% yield loading condition fall in line with the same theoretical curves corresponding to the 80% yield data points, but just slightly more to the left. The data points from the 60% yield loading conditions match up well with the Morrow SG1, SWT SG1, and M-H SG2 theoretical curves.

In comparing the FS experimental results versus the theoretical results from the FS model simulations, the 1B FS experimental data is in much better agreement with the theoretical strain-life results when compared to the results of the 2A FS. The 2A FS experimental data deviated much farther from the corresponding theoretical strain-life curves. The largest deviation of the

experimental data from the theoretical strain-life curves for the 1B FS is rather small when compared to the largest deviation of experimental data to the theoretical curves for the 2A FS. This shows that the 1B FS design is a lot more stable when it comes to characterizing its behavior with fatigue stain-life theory.

Stress concentration factors can be found using charts derived from experimental curve fitting and from finite element analysis. A comparison was done between the stress concentration factors found from the stress concentration chart from Peterson [13] and the ANSYS simulation models to see if the stress concentration factors from both methods were in compliance with each other. The table below shows the stress concentration factors found by the stress concentration chart and the ANSYS simulation models for the 2A and 1B FS geometries.

All of the foregoing analyses have focused on the fatigue behavior of the sensor notched arms. This information is important because it forms the basis for formalizing the life predictions for the base structure (i.e., the structure being monitored) based on the sensor arm failures. Figure 27 shows how, in the simple experiments and analyses employed here, the failure of the sensor elements maps against the predicted failure of the carrier specimen. Clearly, the failures are several orders of magnitude below the predicted structural (CS) life, but the trends are the same. Given what we have learned about predicting the life of a notched sensor arm, it is now conceivable that we can design another set of arm notches that can fill in the life periods at higher cycles. These lives are very hard to replicate experimentally because of their great number, but with properly calibrated simulation models, as our preliminary results indicate, higher range estimates should become possible.

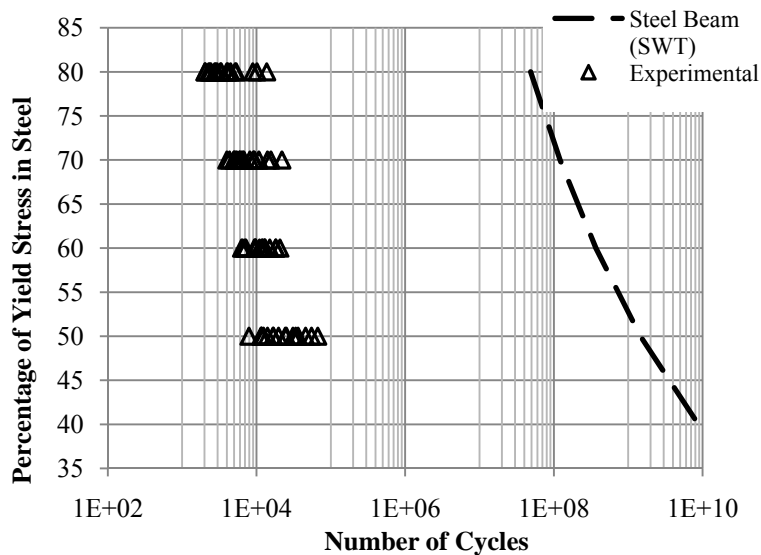


Figure 27: Comparison of experimental notch life and estimated carrier life for constant amplitude loading

5.0 CONCLUDING REMARKS

The experiments and analysis presented here represent the most complete effort to date aimed at conducting a detailed design and performance study on the notch arm fatigue sensor. We obtained reasonable agreement between established strain-life fatigue models and the experimental lives of the sensing elements and showed the connection between the sensor behavior and the life of the underlying structure being monitored.

The deep U-notch prototype developed in this research show promising results towards achieving a final design for an in-situ fatigue sensor. However, there are certain limitations pertaining to the current design that need to be addressed in the future.

- The notch design needs to be further improved to obtain a reasonable gap (cycle-wise) between failures of each notch. This will be helpful in achieving a better coverage of the fatigue life of the monitored structural element.
- Also, the number of sensor arms in the current design can be increased to accommodate additional notches, possibly addressing lower stress ranges with larger number of loading cycles.
- Sensor mounting modification and a size-wise scaling down of the current prototype sensor design will also be necessary to attach them closer to structural details in bridges where high stress concentrations are possible.

6.0 IMPLEMENTATION AND TECHNOLOGY TRANSFER

Given the prototype nature of the fatigue sensor described herein, commercialization of the technology is still in the future. There are still technical problems to be overcome relating to the overestimate of the sensor fatigue damage accumulation, such as the gross section yield in the U-shaped notches, and the surface finish in the notch roots. The latter is the easier to fix, while the former poses a formidable problem in predicting the fatigue life of such dramatically stressed material.

We will continue to seek funding to further the development of fatigue sensing technology, most probably from a more fundamental perspective. The results obtained as part of this study, however, will be invaluable in guiding that research and focusing the problem for potential sponsors.

7.0 REFERENCES

1. "Expanding the Vision of Sensor Materials", Committee on New Sensor Technologies: Materials and Applications, National Materials Advisory Board, Commission on Engineering and Technical Systems, National Research Council, Canada, 1995, pp. 47-61.
2. Lin, M., 1998, *Manufacturing of Composite Structures with a Built-in Network of Piezoceramics*, Ph.D. Dissertation, Department of Mechanical Engineering, Stanford University.
3. Chaudhry, Z., Joseph, T., Sun, F., and Rogers, C., "Local-Area Health Monitoring of Aircraft via Piezoelectric Actuator/Sensor Patches", *Proceedings, SPIE North American Conference on Smart Structures and Materials*, San Diego, CA, 1995.
4. Ihn, Jeong-Beom and Fu-Kuo Chang, "Multi-crack growth monitoring at riveted lap joints using piezoelectric patches", *Proceedings of SPIE, Smart Nondestructive Evaluation for Health Monitoring of Structural and Biological Systems*, March 2002, pp. 29-40.
5. Vodicks, R., 1998, *Use of PVDF Strain Sensors for Health Monitoring of Bonded Composite Patches*, Aeronautical and Maritime Research Lab, Australia.
6. Johnson, P.S., Smith, D.L., and Haugse, E.D., "Characterizing Aircraft High-Cycle Fatigue Environments Using the Damage Dosimeter", Structural Health Monitoring 2000, *Proceedings of the 2nd International Workshop on Structural Health Monitoring*, September 8-10, 1999, Stanford University, CA.
7. Banks, H.T., Inman, D.J., Leo, D.J., Wang, Y., "An Experimentally Validated Damage Detection Theory in Smart Structures", *Journal of Sound and Vibration*, 1996, 191(5), pp. 859-880.
8. Fisher, J. W., Kulak, G. L., Smith, I. F. C., 1998, *Fatigue Primer for Structural Engineers*, National Steel Bridge Alliance, USA.
9. Fisher, J. W., 1984, *Fatigue and Fracture in Steel Bridges - Case Studies*, John Wiley and Sons.
10. Wijesinghe, B.H.M. Priyantha, 2010, *Development of a Prototype In-Situ Fatigue Sensor for Structural Health Monitoring of Highway Bridges*, Ph.D. Dissertation, The University of Oklahoma.
11. Zacharie, S.A., 2009, *In Situ Fatigue Sensor Characterization*, M.S. Thesis, The University of Oklahoma.
12. Endo, T. and Morrow, J., Cyclic Stress-Strain and Fatigue Behavior of Representative Aircraft Metals, *Journal of Materials JMLSA*, 4(1), 1969, pp. 159-175.
13. Pilkey, W.D., 1997, *Peterson's Stress Concentration Factors*, 2ed, John Wiley & Sons.
14. Bannantine, J.A., J.J. Comer and J.L. Handrock, 1990, *Fundamentals of Metal Fatigue Analysis*, Prentice Hall.